CyAbrB2 is a nucleoid-associated protein in *Synechocystis* controlling hydrogenase expression during fermentation

Ryo Kariyazono[1] and Takashi Osanai[1]*

[1]School of Agriculture, Meiji University

*Takashi Osanai

Postal address: 1-1-1 Higashimita, Tama-ku, Kawasaki, Kanagawa 214-8571, Japan

Telephone/Fax: +81-44-934-7103

Email: tosanai@meiji.ac.jp

Author Contributions: RK and TO designed the study; RK performed the study; RK analyzed the data; RK and TO wrote the paper

Competing Interest Statement: The authors declare no conflict of interest.

Keywords: cyanobacteria, transcription, microoxic response, hydrogenase, nucleoid-associated protein, sigma factor

Abstract

The *hox* operon in *Synechocystis* sp. PCC 6803, encoding bidirectional hydrogenase responsible for H_2 production, is transcriptionally upregulated under microoxic conditions. Although several regulators for *hox* transcription have been identified, their dynamics and higher-order DNA structure of *hox* region in microoxic conditions remain elusive. We focused on key regulators for the *hox* operon: cyAbrB2, a conserved regulator in cyanobacteria, and SigE, an alternative sigma factor. Chromatin immunoprecipitation-sequencing revealed that cyAbrB2 binds to the *hox* promoter region under aerobic conditions, with its binding being flattened in microoxic conditions. Concurrently, SigE exhibited increased localization to the *hox* promoter under microoxic conditions. Genome-wide analysis revealed that cyAbrB2 binds broadly to AT-rich genome regions and represses gene expression. Moreover, we demonstrated the physical interactions of the hox promoter region with its distal genomic loci, and the interactions are lowered in microoxic conditions. In the absence of cyAbrB2, the interactions stayed low both in aerobic and microoxic conditions. From these results, we propose that cyAbrB2 is a cyanobacterial nucleoid-associated protein (NAP), modulating chromosomal conformation, which blocks RNA polymerase from the *hox* promoter in aerobic conditions. We further infer that cyAbrB2, with altered localization pattern upon microoxic conditions, modifies chromosomal conformation in microoxic conditions, which allows SigE-containing RNA polymerase to access the *hox* promoter. The coordinated actions of this NAP and the alternative sigma factor are crucial for the proper *hox* expression in microoxic conditions. Our results

33 highlight the impact of cyanobacterial chromosome conformation and NAPs on transcription, which have

34 been insufficiently investigated.

35

36 **Introduction**

37 Cyanobacteria carry out oxygenic photosynthesis but sometimes experience microoxic conditions during

38 the night. Subsequently, cyanobacteria perfrom fermentation, using glycolytic products as electron

39 acceptors. (1). Cyanobacteria have multiple fermentation pathways according to the environment. For

40 example, the freshwater living cyanobacterium *Synechocystis* sp. PCC 6803 (hereafter referred to as

41 *Synechocystis*) produces acetate, lactate, dicarboxylic acids, and hydrogen (1, 2). Genetic manipulations on

42 *Synechocystis* have demonstrated that modulating the expression of certain enzymes can alter fermentative

43 metabolic flow (3, 4). This provides evidence that transcription regulates the fermentative pathway.

44 Hydrogen has attracted significant attention among other cyanobacterial bioproducts owing to its potential

45 as a biofuel. Bidirectional hydrogenase is a key enzyme for H_2 production from protons (5) and is

46 commonly found in cyanobacteria (6). Cyanobacterial hydrogenase comprises five subunits (HoxEFUHY)

47 containing nickel and Fe-S clusters (8). This enzyme can utilize NADH, reduced ferredoxin, and flavodoxin

48 as substrates (7). Hydrogenase can also use excess electrons from the photosynthetic electron transport

49 chain, but photosystem II-generated oxygen can inhibit its activity (9). Another metal-ion-harboring and

50 O_2-sensitive enzyme, pyruvate-ferredoxin oxidoreductase (PFOR), oxidizes pyruvate to produce acetyl-

51 CoA during fermentation. PFOR works coordinatedly with hydrogenase to reduce ferredoxin, which
52 hydrogenase uses as an electron donor (7, 10). Despite their O_2 sensitivity, hydrogenase and PFOR work
53 under mixotrophic (i.e., aerobic) conditions (11, 12). Therefore, uncontrolled expression of *hox* operon and
54 *nifJ* may hamper metabolism under photosynthetic conditions or shorten the supply of inorganic cofactors.
55 Thus, transcriptional regulation in response to the environment is essential for optimal energy cost
56 performance.

57 Promoter recognition by RNA polymerases is an essential step in transcriptional regulation. Sigma factors,
58 subunits of RNA polymerase, recognize core promoter sequences. Transcription factors can also bind to
59 promoter regions to suppress or promote RNA polymerase transcription. As well as recruitment or blocking
60 of RNA polymerase, some transcriptional factors, known as Nucleoid-associated proteins (NAPs),
61 modulate chromosomal conformation to regulate transcription (13). NAPs are common in bacteria, but
62 cyanobacterial NAPs remain unidentified, and higher order of DNA structure in cyanobacteria is yet to be
63 shown. A recent study suggested that the manipulation of chromosomal supercoiling impacts transcriptional
64 properties in cyanobacteria (14). There is room for consideration of NAPs modulating chromosomal
65 conformation and regulating expression in cyanobacteria.

66 In *Synechosysits*, the coding genes of HoxEFUHY form a single operon (sll1220–1226), while PFOR is
67 encoded in the *nifJ* (sll0741) gene. Both *hox* and *nifJ* operons are highly expressed under microoxic
68 conditions (15). Genetic analysis has revealed that multiple global transcriptional regulators control *hox*

69 and *nifJ* expression. Sigma factor SigE (Sll1689) promotes the expression of *hox* and *nifJ* operons (16, 17),

70 while transcription factor cyAbrB2 (Sll0822) represses them (18, 19). Positive regulators for the *hox* operon

71 include LexA (Sll1626) and cyAbrB1 (Sll0359) (20–22).

72 SigE, an alternative sigma factor, controls the expression of genes involved in glycogen catabolism and

73 glycolysis, as well as PFOR/*nifJ* and hydrogenase (16). SigE shares a high amino acid sequence homology

74 with the primary sigma factor SigA, which is responsible for transcribing housekeeping and photosynthetic

75 genes (23). A ChIP-seq study revealed that, while most SigE-binding sites are the same as SigA, SigE

76 exclusively occupies the promoters of glycogen catabolism and glycolysis (24).

77 CyAbrB2 and its homolog cyAbrB1 are transcription factors highly conserved in cyanobacteria. For

78 example, cyAbrB homologs in *Anabaena* sp. PCC7120 is involved in heterocyst formation (25). CyAbrB2

79 in *Synechocystis* regulates the expression of several genes involved in carbon metabolism, nitrogen

80 metabolism, and cell division (19, 26, 27). CyAbrB2 binds to the *hox* promoter *in vitro* and represses its

81 expression *in vivo* (18). CyAbrB1, an essential gene, physically interacts with the CyAbrB2 protein (28)

82 and binds the *hox* promotor region *in vitro* to promote its expression (20).

83 To explore the dynamics of those transcription factors governing the expression of hox operon, we

84 conducted a time-course analysis of the transcriptome and ChIP-seq of SigE and CyAbrB2. Our ChIP-seq

85 and transcriptome analysis showed the NAPs-like nature of cyAbrB2, which prompted us to conduct

86 chromosomal conformation capture assay. 3C analysis revealed the physical interaction between the *hox*

87 promoter region and its downstream and upstream genomic region in the aerobic condition, and that the
88 interaction decreased upon entry to the microoxic condition. Furthermore those interactions in the
89 Δ*cyabrB2* mutant were low both in aerobic and microoxic conditions. From those experiments, we propose
90 that cyAbrB2 modulates chromosomal conformation like NAPs, allowing access to the SigE-containing
91 RNA polymerase complex on the *hox* promoter, by which the *hox* operon achieves distinct expression
92 dynamics. Chromosomal conformation of bacteria is a growing area of interest, and the findings of this
93 study have brought insight into the transcriptional regulation of cyanobacteria.

94 **Results**

95 **Transcriptomes on entry to dark microoxic conditions**

96 To understand transcriptional regulation under microoxic conditions, we conducted a time-course
97 transcriptome capturing aerobic and microoxic conditions at 1-, 2-, and 4-hours timepoints (Figure 1A).
98 Gene set enrichment analysis based on KEGG pathway revealed that many biological pathways, including
99 photosynthesis and respiration (oxidative phosphorylation), were downregulated under microoxic
100 conditions compared to aerobic conditions (Figure 1B). Upregulated pathways included butanoate
101 metabolism and two-component systems, but the actual cyanobacterial catabolic pathway differed slightly
102 from that described in the KEGG pathway. Within 1 hour of switching from aerobic to microoxic conditions,
103 the expression levels of 508 genes increased more than 2-fold. Furthermore, genes with increased
104 expression levels were classified into four based on the time-course (Figure 1C). Of the 508 genes, 28 were

105 termed “transiently upregulated genes” due to their decreased expression upon the comparison of 1- and 4-
106 hours incubation under microoxic conditions (log2 fold change < −0.5), and 119 were termed “continuously
107 upregulated genes.”, which continuously increased between 1- and 4-hours incubation under microoxic
108 conditions (log2-fold change > 0.5). Mapping the classified genes to central carbon metabolism revealed
109 that *nifJ* encoding PFOR and *hox* operon encoding a bidirectional hydrogenase complex were transiently
110 upregulated (Figure 1D and Table 1). RTqPCR verified the transient expression of *hoxF*, *hoxH,* and *nifJ*
111 (Figure S1).

112 **SigE and CyAbrB2 control the expression of transiently upregulated genes**

113 The functional correlation between hydrogenase and PFOR, encoded by the *hox* operon and *nifJ,* suggests
114 that transient upregulation has physiological significance. We focused on transiently upregulated genes and
115 attempted to reveal the regulatory mechanism underlying transient upregulation. While SigE promotes the
116 expression of *hox* and *nifJ*, CyAbrB2 represses them (16, 18, 19). We confirmed that the deletion of *sigE*
117 and *cyabrb2* (Δ*sigE* and Δ*cyabrb2*, respectively) affected the expression of *hoxF*, *hoxH*, and *nifJ* by RT-
118 qPCR (Figure S1). Thus, we conducted a time-course transcriptome analysis of Δ*sigE* and Δ*cyabrb2* under
119 aerobic conditions and after 1- and 2-hours cultivation in dark microoxic conditions (Figures 2A and S2A).
120 The transcriptome data confirmed that SigE and CyAbrB2 regulated *hox* operon expression (Figure 2B).
121 At each time point, we searched for differentially expressed genes (DEGs) between mutants and wildtype
122 with a more than 2-fold expression change and a false discovery rate (FDR) less than 0.05. We found that

123 deleting *sigE* or *cyabrb2* preferentially affected the expression of transiently upregulated genes, not limited

124 to *hox* and *nifJ* operons (Figures 2C and 2D). Interestingly, *cyabrb2* deletion resulted in the upregulated

125 expression of transient genes under aerobic conditions, in contrast to 1-hour cultivation under microoxic

126 conditions (Figure 2C).

127 **Genome-wide analysis of CyAbrB2, CyAbrB1, and SigE via ChIP-seq**

128 To decipher the regulatory mechanism of transiently upregulated genes, we must first comprehend the

129 fundamental features and functions of these transcriptional regulators. Therefore, a genome-wide survey of

130 CyAbrB2 and SigE occupation (Figures S2 and S3) combined with transcriptome data was done.

131 Specifically, we generated a *Synechocystis* strain in which CyAbrB2 was epitope-tagged and performed a

132 ChIP-seq assay under aerobic and microoxic conditions (Figures S2B and S2C). SigE-tagged strains

133 previously constructed and analyzed elsewhere were also employed (24). The primary sigma factor SigA

134 was also analyzed to determine SigE-specific binding. In addition to CyAbrB2, we tagged and analysed

135 CyAbrB1, which is the interactor of CyAbrB2 and positively regulates the *hox* operon.

136 **CyAbrB2 binds to long tracts of the genomic region and suppresses genes in the binding region**

137 The ChIP-seq data showed that CyAbrB2 bound to long tracts of the genomic region with lower GC

138 content than the whole genome *Synechocystis* (Figures 3A and 3B). In addition, regions exhibiting lower

139 GC contents showed a greater binding signal of CyAbrB2 (Figure 3C). This correlation was not a systematic

140 bias of next-generation sequencing because the binding signals of SigE, SigA, and control showed no

141 negative correlation to GC contents (Figure S4A). The binding regions of cyAbrB2 called by peak-caller
142 covered 15.7% of the entire genome length. 805 of 3614 genes overlapped with CyAbrB2 binding regions,
143 and almost half (399 of 805 genes) were entirely covered by CyAbrB2 binding regions. The CyAbrB2
144 binding regions included 80 of 125 insertion sequence elements (Figure 3D). Comparison with the
145 transcriptome of Δ*cyabrB2* revealed CyAbrB2 tended to suppress the genes overlapping with its binding
146 regions under aerobic conditions (Figures 3A and 3E). A survey of the genomic localization of CyAbrB1
147 under aerobic conditions revealed that CyAbrB1 and CyAbrB2 shared similar binding patterns (Figures 3A
148 and S4C). Due to the essentiality of CyAbrB1, we did not perform transcriptome analysis on a CyAbrB1-
149 disrupted strain.

150 **Localization of CyAbrB2 became blurry under the microoxic condition**

151 When cells entered microoxic conditions, the relative binding signals in the CyAbrB2 binding regions
152 slightly declined (Figure S5A). However, the signal change did not necessarily indicate that CyAbrB2
153 binding declined under microoxic conditions because the relative signal was normalized by total
154 immunoprecipitation reads. Rather, the CyAbrB2 binding pattern became uniform when the cells entered
155 microoxic conditions. Notably, the total quantities of precipitated DNA by tagged CyAbrB2 did not
156 decrease, and qPCR confirmed that the CyAbrB2 binding signal increased in all positions tested (Figure
157 S5B and S5C). The protein amount of cyAbrB2 was not altered on entry to the mircooxic condition (Figure
158 S5D).

159 **CyAbrB2 binds to transiently upregulated genes**

160 The binding regions of CyAbrB2 overlapped 17 of 28 transiently upregulated genes, showing significant
161 enrichment from all upregulated genes (Figure 3F). While CyAbrB2 covered the entire length of insertion
162 sequences and unknown proteins, its binding positions on other transient genes were diverse (Figure 3G).
163 Specifically, the *hox* and *nifJ* operons had two distinct binding regions located at the transcription start sites
164 (TSSs) and middle of operons, the *pntAB* operon had two binding regions in the middle and downstream
165 of the operon, and the *nrtABCD* operon had one binding region downstream of the operon (Figure 3H).
166 Upon entry into microoxic conditions, the CyAbrB2 binding signal became less specific, consistent with
167 the general tendency.

168 **Sigma factors SigE and SigA are excluded from CyAbrB2 binding regions regardless of GC contents**

169 We searched for SigE and SigA binding sites under aerobic and microoxic conditions (Figures 4A and 4B,
170 left and right). The SigE and SigA peaks identified in this study predominantly covered the previously
171 identified peaks (Figure S2D), reproducing the previous study's conclusion (24); i.e., SigE and the primary
172 sigma factor SigA share localization on the promoters of housekeeping genes, but SigE exclusively binds
173 to the promoters of its dependent genes. SigE and SigA binding peaks were significantly excluded from the
174 CyAbrB2 binding regions (Figure 4C), and signals in CyAbrB2 binding regions were weaker than those in
175 CyAbrB2-free regions (Figure 4D). As CyAbrB2 prefers AT-rich regions, we examined whether the peak
176 summits of SigE and SigA were located in regions with high GC contents. Unexpectedly, no correlation

177 was found between the GC content and binding signals of SigE and SigA (Figures S4A and S4B). Thus,

178 SigA and SigE are excluded from cyAbrB2 binding regions regardless of GC contents.

179 **Dynamics of sigma factors upon exposure to the microoxic condition**

180 When cells entered microoxic conditions, the binding signals of SigA and SigE were changed, although

181 most of their peaks observed under aerobic conditions were present under microoxic conditions (Figure

182 4A). Next, we focused on sigma factor dynamics in transiently upregulated genes. SigE, but not SigA, binds

183 at the TSS of *pntAB* under aerobic and microoxic conditions (Figure 4E top). Under aerobic conditions,

184 SigE binding summits were not identified at the TSSs of the *hox* and *nifJ* operons. However, the SigE-

185 specific binding summit appeared at the TSS of *nifJ* when cells entered microoxic conditions (Figure 4E

186 middle). A bimodal peak of SigE was observed at the TSS of the *hox* operon, although the peak caller failed

187 to recognize it as two peaks (Figure 4E bottom panel). One side of the bimodal peak near the TSS of the

188 *hox* operon lacked SigA binding. SigE binding without SigA on the promoters of *hox*, *nifj*, and *pntAB* is

189 consistent with their SigE-dependent expression (Figure 2B).

190 **CyAbrB2-dependent and independent chromatin conformation around *hox* operon**

191 We have shown that CyAbrB2 broadly binds to AT-rich genomic regions, including insertion element

192 sequences, and represses expression (Figures 3B and 3D). This is functionally similar to the NAPs (13),

193 which makes us hypothesize that cyAbrB2 modulates chromosomal conformation. Therefore, we

194 conducted the chromatin conformation capture (3C) assay against wildtype and *cyabrb2*Δ strain at aerobic

195 and microoxic conditions (1hr and 4hr). qPCR was performed with unidirectional primer sets, where the

196 genomic fragment containing *hox* operon (hereinafter *hox* fragment) was used as bait (Figure 5A). We then

197 observed that the *hox* fragment interacted with its distal downstream (~25 kbp) region and proximal

198 upstream (~10 kbp) region in the aerobic condition (Figure 5B and 5C, locus(c) and (j)). Those interactions

199 were detected both in wildtype and Δ*cyabrb2*. Moreover, the interaction frequency between the *hox*

200 fragment and its distal downstream was higher in wildtype than Δ*cyabrb2* (Figure S7 locus(c)).

201 **CyabrB2 mediates chromatin conformation changes upon microoxic conditions.**

202 When the wildtype cells entered the microoxic condition, the *hox* fragment diminished its interaction with

203 its distal downstream and proximal upstream region (Figure 5B locus(c) and (j)). By contrast, the interaction

204 frequency in Δ*cyabrb2* mutant were low and unchanged in the aerobic and microoxic conditions. While the

205 interaction scores exhibit considerable variability, the individual data over time demonstrate declining

206 trends of the wildtype at locus (c) and (j) (Figure S7). Furthermore, both wildtype and Δ*cyabrb2* mutant

207 showed increased interaction with the proximal downstream fragments on entry to the microoxic conditions

208 (Figure 5B and 5C, locus (f),(g),(h)). In the wildtype cells, the interaction with locus (g) was transiently

209 elevated at 1 hour of the microoxic condition but decreased to the aerobic level at 4 hours. In summary, 3C

210 analysis demonstrated cyAbrB2-dependent and independent dynamics of chromosomal conformation

211 around the *hox* operon in response to the microoxic condition (Figure 5D).

212 **Discussion**

213 **Physiological significance of transient upregulation of *hox* and *nifJ* operons**

214 The transcriptional upregulation of fermentative genes in response to the microoxic condition is adaptive
215 for energy acquisition. Our time-course transcriptome showed upregulation of several genes involved in
216 catabolism upon exposure to the microoxic condition. The transient upregulation of *hox* and *nifJ* operons
217 is distinctive among them (Figure 1D).

218 The reason for transient upregulation may be the resource constraints of inorganic cofactors and the
219 reusability of fermentative products. Hydrogenase and NifJ proteins have iron–sulfur clusters, and
220 hydrogenase requires nickel for its activity (29, 30). Continuous expression of the *hox* operon should be
221 futile under physiological conditions, as the overexpression of *hoxEFUYH* and *hypABDCEF* (hydrogenase
222 maturation factors) does not yield a proportional increase in hydrogenase activity without an adequate
223 nickel supply (31). Furthermore, hydrogenase-produced H_2 is diffusive and thus difficult to store and reuse
224 as reducing power when cells return to aerobic conditions. Unlike hydrogen fermentation, the reverse
225 tricarboxylic acid (rTCA) cycle produces dicarboxylic acids, which are reusable for generating NADPH
226 via the TCA cycle under aerobic conditions (32). However, adding bicarbonate to phosphoenolpyruvate
227 (PEP) is a rate-limiting step in the rTCA cycle (33). Hydrogenase may favor fermentation initiation since
228 it uses only protons as a substrate, and the rTCA cycle may become active subsequently. In fact, *citH*/*mdh*
229 (sll0891) encoding a key enzyme of the rTCA cycle was classified as continuously upregulated genes in
230 this study (Figure 1D).

231 **Mechanisms for transient expression mediated by SigE and cyAbrB2**

232 SigE and cyAbrB2 can independently contribute to the transient transcriptional upregulation. This is
233 evident as the single mutants, Δ*sigE* or Δ*cyabrb2*, maintained transient expression of *hoxF* and *nifJ* (Figure
234 S1). Here we discuss the cyAbrB2-mediated mechanism, then that of SigE will be discussed.

235 **Three types of the localization pattern and function of cyAbrB2**

236 Herein, we classified three types of binding patterns for cyAbrB2 based on the ChIP-seq data of cyAbrB2.
237 The first is that cyAbrB2 binds a long DNA tract covering the entire gene or operon, represented by the
238 insertion sequence elements. CyAbrB2 suppresses expression in this pattern, as shown in Figures 3D and
239 3E. In the second pattern, cyAbrB2 binds on promoter regions, such as *hox* operon and *nifJ*. Binding on
240 those promoters fluctuates in response to environmental changes, thus regulating expression. This pattern
241 also applies to the promoter of *sbtA* (Na^+/HCO_3^- symporter), as the previous study reported that cyAbrB2
242 is bound to the *sbtA* promoter in a CO_2 concentration-dependent manner (27). The last one is cyAbrB2
243 binding in the middle or downstream of operons. The middle of *hox*, *pntAB*, and *nifJ* operons and the
244 downstream of *nrt* operon are the cases (Figure 3G). Our data show that genes in the same operon separated
245 by the cyAbrB2 binding region behave differently. In particular, *pntB* is classified as the transiently
246 upregulated gene, while *pntA* is not, despite being in the same operon. This might be explained by the recent
247 study which reported that cyAbrB2 affects the stability of mRNA transcribed from its binding gene (34).
248 Hereafter, we will focus on the mechanism of the second pattern, regulation by cyAbrB2 on the promoter.

249 **Insights into transcriptional regulation of *hox* operon and *nifJ***

250 Genome-wide analysis indicates that the CyAbrB2-bound region blocks SigE and SigA (Figures 4C and
251 4D). This is presumably because sigma factors recognize the promoter as a large complex of RNA
252 polymerase. CyAbrB2 binds to the *hox and nifJ* promoter region and may inhibit access to RNA polymerase
253 complex under aerobic conditions. When cells entered microoxic conditions, the binding pattern of
254 cyAbrB2 on the *hox* and *nifJ* promoters got less specific, and SigE binding peaks on those promoters
255 became prominent (Figure 4E). Notably, cyAbrB2 ChIP efficiency at the *hox* promoter is higher in the
256 microoxic condition than in the aerobic condition (Figure S5C). Hence, the mechanism by which cyAbrB2
257 inhibits SigE-containing RNAP in the aerobic condition is not solely based on exclusion by occupancy.
258 Rather, it is plausible that chromosomal conformation change governed by cyAbrB2 provides SigE-
259 containing RNAP with access to the promoter region (Figure 5D).

260 **Chromosomal conformation in *hox* region changes according to the environmental change**

261 3C analysis demonstrated the interaction between the *hox* promoter and its distal genomic region, which
262 decreased on entry to the microoxic condition. CyAbrB2 mediates the interaction between the hox fragment
263 and the distal downstream region. The observed conformational change correlates with the expression of
264 the *hox* operon, though further investigations are needed to establish causality (Figures 5B and S7, locus
265 (f), (g), and (j)). A recent study demonstrated that manipulating the expression of topoisomerase, which
266 influence chromosomal conformational change through supercoiling, affect transcriptional properties in

267 cyanobacteria (14). Moreover, Song et al. pointed out that DNA looping may inhibit transcription in
268 cyanobacteria (34) because artificial DNA looping by the LacI repressor of *E. coli* can repress
269 cyanobacterial transcription (35). Thus, we infer conformation change detected by the present 3C
270 experiment regulates expression of *hox* operon.

271 **A possible mechanism for cyAbrB2-mediated chromosomal conformation**

272 The *hox* promoter region possesses the cyAbrB2 binding region, and locus (c) is adjacent to the cyAbrB2
273 binding region. Consequently, cyAbrB2 may mediate chromosomal conformation by bridging its binding
274 regions, as other NAPs do. However, no biochemical data mentioned the DNA bridging function of
275 cyAbrB2 in the previous studies (18, 26, 34). CyAbrB1, the homolog of cyAbrB2, may cooperatively work,
276 as cyAbrB1 directly interacts with cyAbrB2 (28), and their distribution is similar (Figure 3A). In the
277 microoxic condition, cyAbrB2 binding became blurry, which might reduce the specific interaction between
278 the hox region and locus (c). On the other hand, cyAbrB2 indirectly mediates interaction with its proximal
279 upstream region (Figure 5B, locus (j)), as this region is devoid of cyAbrB2 binding (Figure 5A locus (i) to
280 (l)).

281 **Generality for chromosomal conformation in cyanobacteria**

282 Our 3C analysis revealed that local chromosomal conformation changes upon entry to the microoxic
283 conditions (Figure 5). The conformational changes occur in both AbrB2-dependent and AbrB2-independent
284 manners. Cyanobacteria face various environmental changes besides the microoxic condition, and there are

285 potential NAPs in cyanobacteria yet to be characterized. It is speculated that conformational change of the

286 entire chromosome occurs to deal with many environmental stresses.

287 **The sigE-mediated mechanism for the transient expression**

288 One possible SigE-mediated mechanism for transient expression is the post-transcriptional activation and

289 degradation of SigE in the dark; i.e., SigE is sequestered by binding to the H subunit of Magnesium-

290 chelatase under light conditions and released under dark (36), enabling acute transcription of *hox* operon

291 and *nifJ*. Transcripts of *sigE* were continuously downregulated in our time-course transcriptome, while *sigB*

292 (sll0306) and *sigC* (sll0184) were classified as continuous upregulated genes (Supplemental Table S1). It

293 is possible that upregulated SigB and SigC outcompete SigE in prolonged incubation under microoxic

294 conditions. Finally, SigE is degraded under dark within 24 hours (37).

295 Another reason for the microoxic specific expression may exist in the sequence of the *hox* promoter. We

296 previously determined the consensus sequence of -10 element for SigE regulon in the aerobic condition as

297 "TANNNT," where N is rich in cytosine (24). The -10 sequence of the *hox* promoter "TAACAA" (22)

298 deviates from the consensus, and no hexamer precisely fitting the consensus are found in the *nifJ* promoter.

299 This deviation can inhibit SigE from binding during aerobic conditions, aside from cyAbrB2-mediated

300 inhibition. Under the microoxic condition, transcription factors LexA (22) and Rre34 (15) may aid SigE

301 binding to the promoter of *hox* and *nifJ*, respectively. Overall, multiple environmental signals are integrated

302 into the *hox* and *nifJ* promoter through the CyAbrB2 and SigE dynamics.

303 **Materials and Methods**

304 **Bacterial strains and plasmids**

305 The glucose-tolerant strain of *Synechocystis* sp. PCC 6803 (38) was used as a wildtype strain in this study.

306 The *sigE* (sll1689)-disrupted strain (G50) was constructed in a previous study (16). Disruption and epitope-

307 tagging of *cyabrb1*(sll0359) and *cyabrb2*(sll0822) were performed by homologous double recombination

308 between the genome and PCR fragment (38). The resulting transformants were selected using three

309 passages on BG-11 plates containing 5 µg/mL kanamycin. Genomic PCR was used to confirm the insertion

310 of epitope tag fragments and gene disruption (Figure S2A). Supplemental Tables S2, S3, and S4 contain

311 the cyanobacterial strains, oligonucleotides, and plasmids used in this study.

312 **Aerobic and microoxic culture conditions**

313 For aerobic conditions, cells were harvested after 24 hours cultivation in HEPES-buffered BG-11_0 medium

314 (39), which was buffered with 20 mM HEPES-KOH (pH 7.8) containing 5 mM NH_4Cl under continuous

315 exposure to white light (40 µmol $m^{-2}s^{-1}$) and bubbled with air containing 1% CO_2 (final OD_{730} = 1.4–1.8).

316 For the dark microoxic culture, the aerobic culture cell was concentrated to an OD_{730} of 20 with the

317 centrifuge and resuspended in the culture medium. The concentrated cultures were poured into vials,

318 bubbled with N_2 gas, and sealed. The sealed vials were shaded and shaken at 30˚C for the described times.

319 **Antibodies and immunoblotting**

320 Sample preparation for immunoblotting was performed as previously described (24), and FLAG-tagged

321 proteins were detected by alkaline-phosphatase-conjugated anti-FLAG IgG (A9469, Sigma Aldrich, St.
322 Louis, MO) and 1-Step NBT/BCIP substrate solution (Thermo Fisher Scientific, Waltham, MA).

323 **RNA isolation**

324 Total RNA was isolated with ISOGEN (Nippon gene, Tokyo, Japan) following the manufacturer's
325 instructions and stored at −80˚C until use. The extracted RNA was treated with TURBO DNase (Thermo
326 Fisher Scientific) for 1 hour at 37˚C to remove any genomic DNA contamination. We confirmed that the
327 A260/A280 of the extracted RNA was >1.9 by NanoDrop Lite (Thermo Fisher Scientific). We prepared
328 triplicates for each timepoint for the RNA-seq library. RT-qPCR was performed as discribed elsewhere (37).

329 **ChIP assay**

330 Two biological replicates were used for each ChIP-seq experiment, and one untagged control ChIP was
331 performed. ChIP and qPCR analyses were performed using the modified version of a previous method (24).
332 FLAG-tagged proteins were immunoprecipitated with FLAG-M2 antibody (F1804 Sigma-Aldrich)
333 conjugated to protein G dynabeads (Thermo Fisher Scientific).

334 **Library preparation and next-generation sequencing**

335 For the ChIP-seq library, input and immunoprecipitated DNA were prepared into multiplexed libraries
336 using NEBNext Ultra II DNA Library Prep Kit for Illumina (New England Biolabs, Ipswich, MA). For the
337 RNA-seq library, isolated RNA samples were deprived of ribosomal RNA with Illumina Ribo-Zero Plus
338 rRNA Depletion Kit (Illumina, San Diego, CA) and processed into a cDNA library for Illumina with the

339 NEBNext Ultra II Directional RNA Library Prep Kit for Illumina (New England Biolabs). Dual-index
340 primers were conjugated with NEBNext Multiplex Oligos for Illumina (Set1, New England Biolabs). We
341 pooled all libraries, and the multiplexed libraries were dispatched to Macrogen Japan Inc. and subjected to
342 paired-end sequencing with HiSeqX. Adapter trimming and quality filtering of raw sequence reads were
343 conducted with fastp (ver. 0.21.0) (40) under default conditions. The paired-end sequences were mapped
344 onto the *Synechocystis* genome (ASM972v1) using Bowtie2 (41) (ver. 2.4.5 paired-end). Supplementary
345 Table S5 contains the read counts that passed via fastp quality control and were mapped by Bowtie2.

346 **RNA-seq analysis**

347 Mapped reads were counted by HT-seq count (ver. 2.0.2) (42) for the GFF file of ASM972v1, with the
348 reverse-strandedness option. EdgeR package (ver. 3.40.1) (43) was used to perform the differential
349 expression analysis. Fold changes in expression and FDR were used for gene classification. Supplemental
350 Table S6-S8 contains fold change in gene expression calculated by edgeR.

351 **Genome-wide analyses**

352 Peaks were called using the MACS3 program (ver. 3.0.0b1) (44). For paired-end reads for SigE, SigA,
353 and untagged control ChIP, narrow peaks were called with <1e−20 of the q-value cut-off and "--call-
354 summits" options. The peak summits from two replicates and the untagged control were merged if summits
355 were located within 40 bp of each other. Peak summits identified in both replicates but not in the control,
356 were considered for further analysis. The midpoint of the peak summits for the two merged replicates was

357 further analyzed.

358 Broad peak calling methods were applied to paired-end reads for CyAbrB2, CyAbrB1, and untagged

359 control ChIP using the "–broad" option, with a q-value cut-off of < 0.05 and a q-value broad cut-off of <

360 0.05. The intersection of broad peaks from two replicates, excluding those called by the control, was used

361 in subsequent analyses.

362 The positions of the TSS, including internal start sites, were obtained as reported by Kopf et al. [45]. The read

363 count, merging, and the intersection of the binding region were calculated using BEDTools (ver. 2.30.0)

364 (46). Supplemental Tables S9–S15 contain SigA and SigE peaks and the broad binding regions of CyAbrB2

365 and CyAbrB1, respectively.

366 Binding signals in every 100 bp bin for scatter plots were calculated as (IP read counts within 100 bp

367 window) / (input read counts within 100 bp window) * (total input read counts/total IP read counts). GC

368 contents were calculated within 500 bp in 100 bp sliding windows by seqkit (ver. 2.3.0) (47).

369 **Genome extraction, digestion, and ligation for 3C assay**

370 A 3C assay was conducted based on the previous prokaryotic Hi-C experiment (48, 49), with certain steps

371 modified. To begin, *Synechocystis* were fixed with 2.5% formaldehyde for 15 minutes at room temperature.

372 Fixation was terminated by adding a final concentration of 0.5M of glycine, and cells were stored at -80˚C

373 until use. Fixed cells were disrupted using glass beads and shake master NEO (Bio Medical Science, Tokyo,

374 Japan), following the previous study's instructions for preparing cell lysate for ChIP. The lysates were

375 incubated with buffer containing 1mM Tris-HCl (pH7.5), 0.1mM EDTA, and 0.5% SDS for 10min at room
376 temperature, and 1% Triton X-100 quenched SDS. Genomes in the cell lysate were digested by 600U/mL
377 of HindIII (Takara Bio, Shiga, Japan) for 4 hours at 37˚C, and RNA in the lysate was simultaneously
378 removed by 50 µg/mL of RNaseA (Nippon genetics, Tokyo, Japan). The digestion was terminated by adding
379 1% SDS and 22 mM EDTA. The fill-in reaction and biotin labeling steps were omitted from the procedure.
380 The digested genomes were diluted by ligation buffer containing 1% triton-X100 to the final concentration
381 of approximately 1µg/mL and incubated for 10 min at room temperature. Ligation was performed with 2
382 U/mL of T4 DNA ligase (Nippon Gene) overnight at 16˚C. Crosslinking was reversed under 65˚C for 4
383 hours in the presence of 2.5 mg/mL of proteinase K (Kanto Chemical, Tokyo, Japan), and DNA was purified
384 with the phenol-chloroform method and ethanol precipitation method.

385 **Preparation of calibration samples for 3C qPCR**

386 Based on a previous study, calibration samples for possible ligated pairs were prepared in parallel with 3C
387 ligation (50). In brief, the purified genome of *Synechocystis* was digested by HindIII, and DNA was purified
388 with the phenol-chloroform and ethanol precipitation. Purified DNA was dissolved into the ligation buffer
389 at a concentration of about 600ng/µL and ligated with 2 U/mL of T4 DNA ligase at 16˚C overnight. As a
390 result, DNA ~600-fold condensed DNA than 3C samples were ligated.

391 **Quantification of crosslinking frequency for 3C assay**

392 Before the real-time PCR assay, we confirmed that each primer set amplified single bands in a ligation-

393 dependent manner by GoTaq Hot Start Green Master Mix (Promega, Madison, WI) (Figure S6). Real-time
394 PCR was performed with StepOnePlus (Applied Biosystems, Foster City, CA) and Fast SYBR Green
395 Master Mix (Thermo Fisher Scientific) according to the manufacturer's instructions. Interaction frequency
396 was calculated by ΔΔCt method using dilution series of calibration samples described above. We confirmed
397 each primer set amplified DNA fragment with a unique Tm value. The amount of the bait fragment
398 containing *hox* operon were quantified and used as an internal control. Supplemental Table S4 contains the
399 list of primers used in the 3C quantification. Interaction frequency for each primer position was calculated
400 as the relative abundance of ligated fragments against the calibration samples and normalized among
401 samples by internal control.

402 **Statistical analysis**

403 Statistical analyses were performed with R version 4.2.2 (51). The "fisher.test" function was used for
404 Fisher's exact test, and p-values < 0.05 were denoted as asterisks in the figure. Multiple comparisons of
405 Fisher's exact test were conducted using "fisher. Multcomp" function in the RVAideMemoire package (52),
406 where P-values were adjusted by the "fdr" method and FDRs <0.05 are shown in the figures. Multiple
407 comparisons of the Wilcoxon-rank test were conducted by "pairwise.wilcox.test," and p-values were
408 adjusted by the "fdr" method. Adjusted p-values < 0.05 are shown in the figure. The correlation coefficient
409 was calculated with the "cor" function. Gene set enrichment analysis (GSEA) was performed by
410 culsterPlofiler package (53) in R with p-value cut-off of 0.05. The enriched pathways detected by GSEA

are listed in Supplemental Table S16.

Manuscript writing

We employed GPT-3.5 to refine the expression of the manuscripts.

Accession Numbers

Raw ChIP sequencing and RNA sequencing reads were deposited in the Sequence Read Archive (accession ID: PRJNA956842).

Declaration of interest

The authors declare no competing interests.

Acknowledgments

This study was supported by the following grants to T.O.: Grant-in-Aid for Scientific Research (B) (grant no. 20H02905), JST-ALCA of the Japan Science and Technology Agency (grant number JPMJAL1306), and the Asahi Glass Foundation. We thank Dr. Kohki Yoshimoto for providing laboratory instruments and Ms. Kaori Iwazumi for the support of bacterial culture and the medium preparation.

Author contributions

R.K. and T.O. designed the study; R.K. conducted the experiment; R.K. analyzed the data; R.K. and T.O. wrote the paper.

429 **References**

430 1. L. J. Stal, R. Moezelaar, Fermentation in cyanobacteria1Publication 2274 of the Centre of

431 Estuarine and Coastal Ecology, Yerseke, The Netherlands.1. *FEMS Microbiol. Rev.* **21**, 179–211

432 (1997).

433 2. T. Osanai, *et al.*, Genetic manipulation of a metabolic enzyme and a transcriptional regulator

434 increasing succinate excretion from unicellular cyanobacterium . *Front. Microbiol.* **6**, 1064

435 (2015).

436 3. H. Iijima, *et al.*, Four-carbon dicarboxylic acid production through the reductive branch of the

437 open cyanobacterial tricarboxylic acid cycle in *Synechocystis* sp. PCC 6803. *Metab. Eng.* **65**, 88–

438 98 (2021).

439 4. H. Iijima, *et al.*, Metabolomics-based analysis revealing the alteration of primary carbon

440 metabolism by the genetic manipulation of a hydrogenase HoxH in *Synechocystis* sp. PCC 6803.

441 *Algal Res.* **18**, 305–313 (2016).

442 5. D. Carrieri, K. Wawrousek, C. Eckert, J. Yu, P.-C. Maness, The role of the bidirectional

443 hydrogenase in cyanobacteria. *Bioresour. Technol.* **102**, 8368–8377 (2011).

444 6. V. Puggioni, S. Tempel, A. Latifi, Distribution of Hydrogenases in Cyanobacteria: A Phylum-

445 Wide Genomic Survey. *Front. Genet.* **7**, 223 (2016).

446 7. K. Gutekunst, *et al.*, The bidirectional NiFe-hydrogenase in *Synechocystis* sp. PCC 6803 is

447 reduced by flavodoxin and ferredoxin and is essential under mixotrophic, nitrate-limiting
448 conditions. *J. Biol. Chem.* **289**, 1930–1937 (2014).
449 8. C. Cassier-Chauvat, T. Veaudor, F. Chauvat, Advances in the function and regulation of
450 hydrogenase in the cyanobacterium *Synechocystis* PCC6803. *Int. J. Mol. Sci.* **15**, 19938–19951
451 (2014).
452 9. J. Appel, S. Phunpruch, K. Steinmüller, R. Schulz, The bidirectional hydrogenase of
453 *Synechocystis* sp. PCC 6803 works as an electron valve during photosynthesis. *Arch. Microbiol.*
454 **173**, 333–338 (2000).
455 10. J. H. Artz, *et al.*, The structure and reactivity of the HoxEFU complex from the cyanobacterium
456 *Synechocystis* sp. PCC 6803. *J. Biol. Chem.* **295**, 9445–9454 (2020).
457 11. Y. Wang, *et al.*, Pyruvate:ferredoxin oxidoreductase and low abundant ferredoxins support
458 aerobic photomixotrophic growth in cyanobacteria. *Elife* **11**, 2021.08.27.457892 (2022).
459 12. H. Burgstaller, *et al.*, *Synechocystis* sp. PCC 6803 Requires the Bidirectional Hydrogenase to
460 Metabolize Glucose and Arginine Under Oxic Conditions. *Front. Microbiol.* **13**, 896190 (2022).
461 13. J. Hołówka, J. Zakrzewska-Czerwińska, Nucleoid Associated Proteins: The Small Organizers
462 That Help to Cope With Stress. *Front. Microbiol.* **11**, 590 (2020).
463 14. A. Behle, *et al.*, Manipulation of topoisomerase expression inhibits cell division but not growth
464 and reveals a distinctive promoter structure in Synechocystis. *Nucleic Acids Res.* **50**, 12790–

465 12808 (2022).

466 15. T. C. Summerfield, S. Nagarajan, L. A. Sherman, Gene expression under low-oxygen conditions

467 in the cyanobacterium *Synechocystis* sp. PCC 6803 demonstrates Hik31-dependent and -

468 independent responses. *Microbiology* **157**, 301–312 (2011).

469 16. T. Osanai, *et al.*, Positive regulation of sugar catabolic pathways in the cyanobacterium

470 *Synechocystis* sp. PCC 6803 by the group 2 sigma factor sigE. *J. Biol. Chem.* **280**, 30653–30659

471 (2005).

472 17. T. Osanai, *et al.*, Genetic engineering of group 2 sigma factor SigE widely activates expressions

473 of sugar catabolic genes in *Synechocystis* species PCC 6803. *J. Biol. Chem.* **286**, 30962–30971

474 (2011).

475 18. J. Dutheil, *et al.*, The AbrB2 autorepressor, expressed from an atypical promoter, represses the

476 hydrogenase operon to regulate hydrogen production in *Synechocystis* strain PCC6803. *J.*

477 *Bacteriol.* **194**, 5423–5433 (2012).

478 19. C. Leplat, *et al.*, Genome-wide transcriptome analysis of hydrogen production in the

479 cyanobacterium Synechocystis: Towards the identification of new players. *Int. J. Hydrogen*

480 *Energy* **38**, 1866–1872 (2013).

481 20. P. Oliveira, P. Lindblad, An AbrB-Like protein regulates the expression of the bidirectional

482 hydrogenase in *Synechocystis* sp. strain PCC 6803. *J. Bacteriol.* **190**, 1011–1019 (2008).

483 21. K. Gutekunst, *et al.*, LexA regulates the bidirectional hydrogenase in the cyanobacterium
484 *Synechocystis* sp. PCC 6803 as a transcription activator. *Mol. Microbiol.* **58**, 810–823 (2005).
485 22. P. Oliveira, P. Lindblad, LexA, a transcription regulator binding in the promoter region of the
486 bidirectional hydrogenase in the cyanobacterium *Synechocystis* sp. PCC 6803. *FEMS Microbiol.*
487 *Lett.* **251**, 59–66 (2005).
488 23. S. Imamura, M. Asayama, Sigma factors for cyanobacterial transcription. *Gene Regul. Syst. Bio.*
489 **3**, 65–87 (2009).
490 24. R. Kariyazono, T. Osanai, Identification of the genome-wide distribution of cyanobacterial group-
491 2 sigma factor SigE, accountable for its regulon. *Plant J.* **110**, 548–561 (2022).
492 25. A. Higo, E. Nishiyama, K. Nakamura, Y. Hihara, S. Ehira, cyAbrB Transcriptional Regulators as
493 Safety Devices To Inhibit Heterocyst Differentiation in Anabaena sp. Strain PCC 7120. *J.*
494 *Bacteriol.* **201** (2019).
495 26. A. Ishii, Y. Hihara, An AbrB-like transcriptional regulator, Sll0822, is essential for the activation
496 of nitrogen-regulated genes in *Synechocystis* sp. PCC 6803. *Plant Physiol.* **148**, 660–670 (2008).
497 27. J. Lieman-Hurwitz, *et al.*, A cyanobacterial AbrB-like protein affects the apparent photosynthetic
498 affinity for CO2 by modulating low-CO2-induced gene expression. *Environ. Microbiol.* **11**, 927–
499 936 (2009).
500 28. Y. Yamauchi, Y. Kaniya, Y. Kaneko, Y. Hihara, Physiological roles of the cyAbrB

501 transcriptional regulator pair Sll0822 and Sll0359 in *Synechocystis* sp. strain PCC 6803. *J.*
502 *Bacteriol.* **193**, 3702–3709 (2011).
503 29. K. Uyeda, J. C. Rabinowitz, Pyruvate-ferredoxin oxidoreductase. 3. Purification and properties of
504 the enzyme. *J. Biol. Chem.* **246**, 3111–3119 (1971).
505 30. P. M. Vignais, B. Billoud, Occurrence, classification, and biological function of hydrogenases: an
506 overview. *Chem. Rev.* **107**, 4206–4272 (2007).
507 31. M. Ortega-Ramos, *et al.*, Engineering *Synechocystis* PCC6803 for hydrogen production:
508 influence on the tolerance to oxidative and sugar stresses. *PLoS One* **9**, e89372 (2014).
509 32. N. Katayama, K. Iwazumi, H. Suzuki, T. Osanai, S. Ito, Malic Enzyme, not Malate
510 Dehydrogenase, Mainly Oxidizes Malate That Originates from the Tricarboxylic Acid Cycle in
511 Cyanobacteria. *MBio* **13**, e0218722 (2022).
512 33. T. Hasunuma, M. Matsuda, A. Kondo, Improved sugar-free succinate production by
513 *Synechocystis* sp. PCC 6803 following identification of the limiting steps in glycogen
514 catabolism. *Metab. Eng. Commun.* **3**, 130–141 (2016).
515 34. K. Song, *et al.*, Expression of the Cyanobacterial F(o)F(1) ATP Synthase Regulator AtpΘ
516 Depends on Small DNA-Binding Proteins and Differential mRNA Stability. *Microbiol. Spectr.*
517 **10**, e0256221 (2022).
518 35. D. Camsund, T. Heidorn, P. Lindblad, Design and analysis of LacI-repressed promoters and

519 DNA-looping in a cyanobacterium. *J. Biol. Eng.* **8**, 4 (2014).

520 36. T. Osanai, *et al.*, ChlH, the H subunit of the Mg-chelatase, is an anti-sigma factor for SigE in

521 *Synechocystis* sp. PCC 6803. *Proc. Natl. Acad. Sci. U. S. A.* **106**, 6860–6865 (2009).

522 37. H. Iijima, *et al.*, Changes in primary metabolism under light and dark conditions in response to

523 overproduction of a response regulator RpaA in the unicellular cyanobacterium *Synechocystis* sp.

524 PCC 6803 . *Front. Microbiol.* **6**, 888 (2015).

525 38. J. G. K. Williams, "Construction of Specific Mutations in Photosystem II Photosynthetic

526 Reaction Center by Genetic Engineering Methods in *Synechocystis* 6803" in *Methods in*

527 *Enzymology*, (Academic Press, 1988), pp. 766–778.

528 39. R. Rippka, J. Deruelles, J. B. Waterbury, Generic assignments, strain histories and properties of

529 pure cultures of cyanobacteria. *J. Gen. Microbiol.* **111**, 1–61 (1979).

530 40. S. Chen, Y. Zhou, Y. Chen, J. Gu, fastp: an ultra-fast all-in-one FASTQ preprocessor.

531 *Bioinformatics* **34**, i884–i890 (2018).

532 41. B. Langmead, S. L. Salzberg, Fast gapped-read alignment with Bowtie 2. *Nat. Methods* **9**, 357–

533 359 (2012).

534 42. S. Anders, P. T. Pyl, W. Huber, HTSeq--a Python framework to work with high-throughput

535 sequencing data. *Bioinformatics* **31**, 166–169 (2015).

536 43. M. D. Robinson, D. J. McCarthy, G. K. Smyth, edgeR: a Bioconductor package for differential

537 expression analysis of digital gene expression data. *Bioinformatics* **26**, 139–140 (2010).

538 44. Y. Zhang, *et al.*, Model-based analysis of ChIP-Seq (MACS). *Genome Biol.* **9**, R137 (2008).

539 45. M. Kopf, *et al.*, Comparative genome analysis of the closely related *Synechocystis* strains PCC

540 6714 and PCC 6803. *DNA Res.* **21**, 255–266 (2014).

541 46. A. R. Quinlan, I. M. Hall, BEDTools: a flexible suite of utilities for comparing genomic features.

542 *Bioinformatics* **26**, 841–842 (2010).

543 47. W. Shen, S. Le, Y. Li, F. Hu, SeqKit: A Cross-Platform and Ultrafast Toolkit for FASTA/Q File

544 Manipulation. *PLoS One* **11**, e0163962 (2016).

545 48. N. Takemata, R. Y. Samson, S. D. Bell, Physical and Functional Compartmentalization of

546 Archaeal Chromosomes. *Cell* **179**, 165-179.e18 (2019).

547 49. N. Takemata, S. D. Bell, Chromosome conformation capture assay combined with biotin

548 enrichment for hyperthermophilic archaea. *STAR Protoc.* **2**, 100576 (2021).

549 50. M. Abou El Hassan, R. Bremner, A rapid simple approach to quantify chromosome conformation

550 capture. *Nucleic Acids Res.* **37**, e35 (2009).

551 51. , R: A Language and Environment for Statistical Computing (2022).

552 52. M. Hervé, RVAideMemoire: Testing and Plotting Procedures for Biostatistics (2022).

553 53. T. Wu, *et al.*, clusterProfiler 4.0: A universal enrichment tool for interpreting omics data. *Innov.*

554 *(Cambridge* **2**, 100141 (2021).

555

556 **Table 1** List of transiently upregulated genes

		Operon
Oxidoreductase		
sll0741	*nifJ*/"pyruvate-ferredoxin/flavodoxin oxidoreductase"	TU3296
sll0743	hypothetical protein	
sll0744	dihydroorotate dehydrogenase (fumarate)	
sll1221	*hoxF*/“bidirectional [NiFe] hydrogenase diaphorase subunit”	TU1714
sll1222	unknown protein	
sll1223	*hoxU*/“bidirectional [NiFe] hydrogenase diaphorase subunit”	
sll1224	*hoxY*/“NAD-reducing hydrogenase small subunit”	
sll1225	unknown protein	
sll1226	*hoxH*/“NAD-reducing hydrogenase large subunit”	
slr1434	*pntB*/"H+-translocating NAD(P) transhydrogenase subunit beta"	TU1089
Transporter		
sll1450	*nrtA*/“nitrate/nitrite transport system substrate-binding protein”	TU1023
sll1451	*nrtB*/“nitrate/nitrite transport system permease protein”	
sll1452	*nrtC*/“nitrate/nitrite transport system ATP-binding protein”	
sll1453	*nrtD*/“nitrate/nitrite transport system ATP-binding protein”	
Two-component system		
slr1214	twitching motility two-component system response regulator PilG	TU905
slr1215	unknown protein	TU907
Glycosyl transferase		
slr2116	*spsA*/“spore coat polysaccharide biosynthesis protein; SpsA”	TU1673

Protease		
sll1009	*frpC*/"iron-regulated protein"	TU491
Insertion sequence (Transposase)		
slr1523	transposase	TU1659
sll1985	transposase	TU1589
sll7001	transposase	NA
sll7003	toxin FitB	TU7001
ssl0172	transposase	TU3163
Other		
slr1260	hypothetical protein	TU1446
slr0668	unknown protein	TU3532
slr5127	unknown protein	TU5127
sll0710	unknown protein	TU97
sll1307	unknown protein	TU1224

557 The list of transiently upregulated genes was merged by transcriptional units and sorted by function. The

558 transcriptional unit information was obtained from a previous study (Kopf et al., 2014).

559

560

561 **Figures and Figure legends**

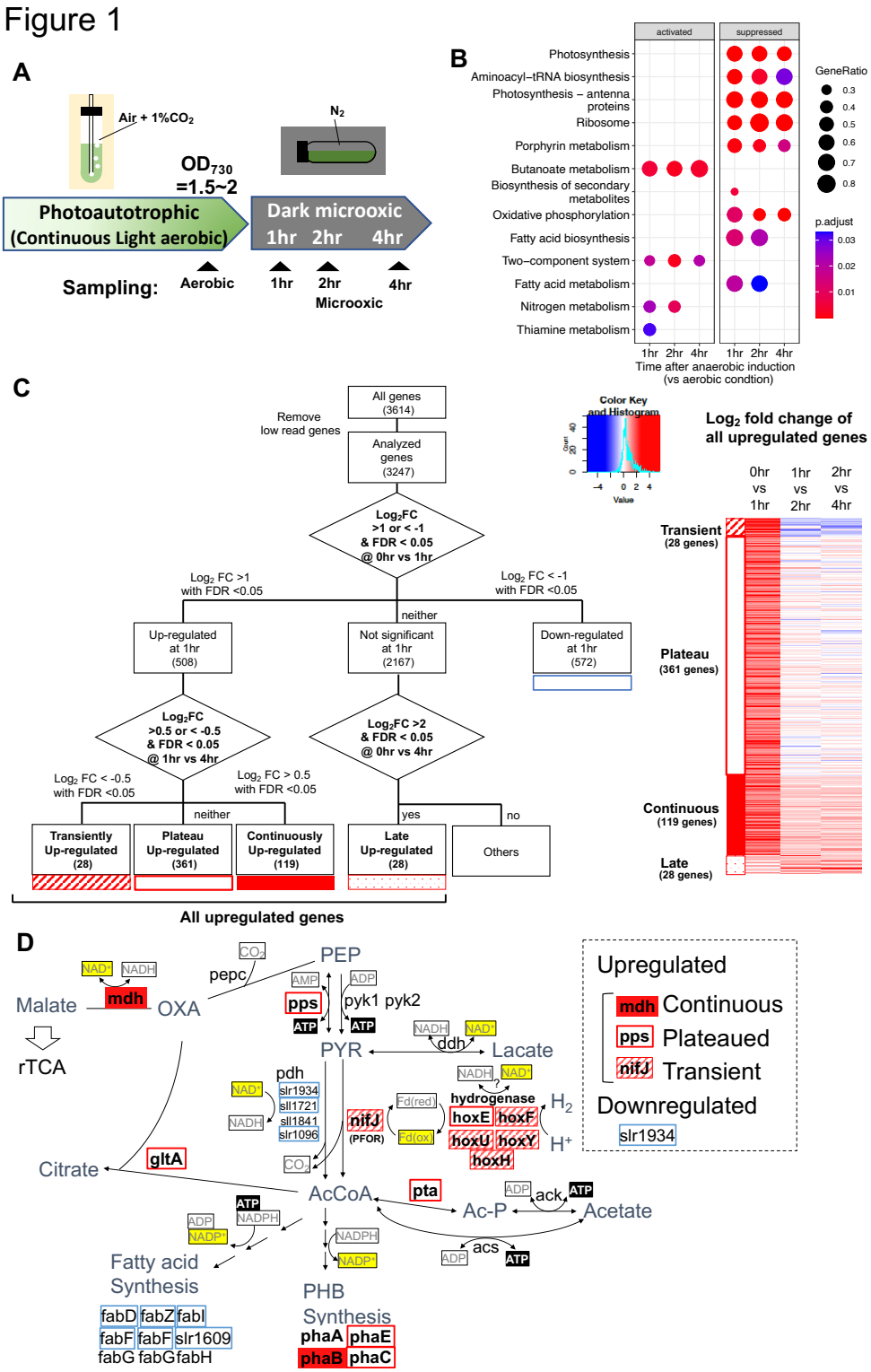

562

563 **Figure 1**

564 (A) Schematic diagram for the sampling of cells under aerobic and microoxic conditions. (B) Gene set
565 enrichment analysis on time-course transcriptome data. KEGG pathways enriched in upregulated or
566 downregulated genes after 1-, 2-, and 4-h incubation under microoxic conditions are shown. (C) (left)
567 Schematic diagram showing the classification of genes according to the time-course transcriptome.
568 Transient (striped square), Plateau (open square), Continuous (filled square), and Late (dotty square) are
569 denoted as all upregulated genes. (right) Heatmap showing expression change in all upregulated genes
570 over the time-course. Genes were clustered into subgroups and sorted by the gene name. (D) The
571 classified genes were mapped to the central carbon metabolism, centered on pyruvate. PEP:
572 phosphoenolpyruvate, PYR: pyruvate, AcCoA: acetyl CoA, Ac-P: acetyl phosphate, OXA: oxaloacetate,
573 PHB: polyhydroxy butyrate. rTCA: reverse tricarboxylic acid cycle.
574

Figure 2

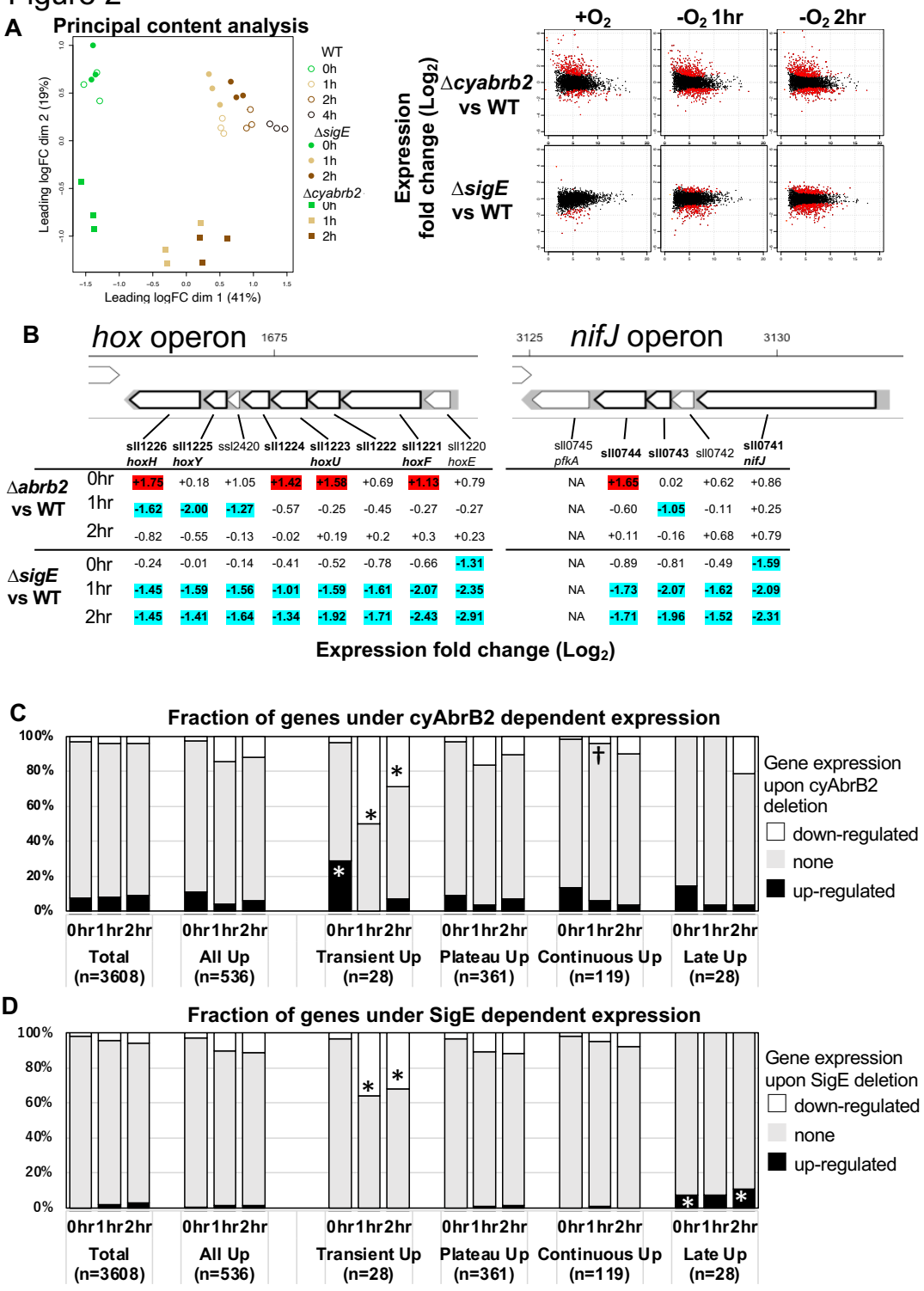

575

576 **Figure 2**

577 (A) (left) Primary component scatter plot showing the profiles of RNA-seq data. (right) MA plot showing

578 fold change (y-axis) and average (x-axis) of gene expression between wildtype and mutant strains at each

579 timepoint. Red dots indicate defined DEGs (|Log_2 FC| >1 with FDR < 0.05). (B) Log2 scaled expression

580 fold change in genes in the *hox* and *nifJ* operons upon Δ*cyabrb2* and Δ*sigE* under aerobic conditions (0

581 h), 1 hour after anoxic condition (1 hr), and 2 hours after anoxic condition (2 hr). DEGs are marked with

582 sky blue (downregulated upon deletion) or red (upregulated upon deletion). (C and D) Fraction of

583 upregulated and downregulated genes upon the (C) Δ*cyabrb2* and (D) Δ*sigE* at the timepoints of aerobic

584 conditions (0 hr), 1 hour after anoxic condition (1 hr), and 2 hour after anoxic condition (2 hr). Genes are

585 classified according to Figure 1C. Asterisk (*) and dagger (†) denote statistically significant enrichment

586 and anti-enrichment compared with all upregulated genes tested by multiple comparisons of Fisher's

587 exact test (FDR < 0.05).

588

Figure 3

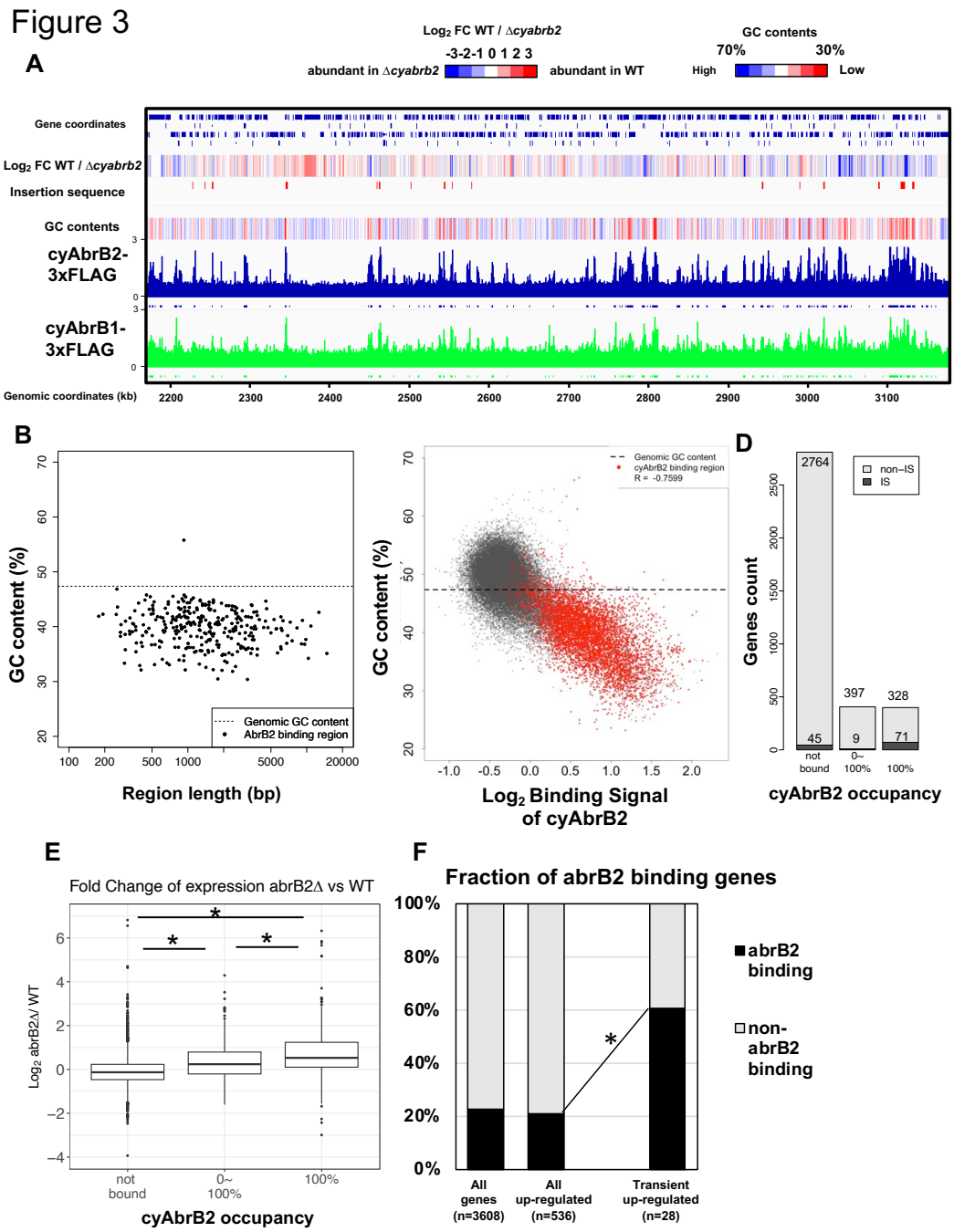

Figure 3 (continuing)

Figure 3 (continuing)

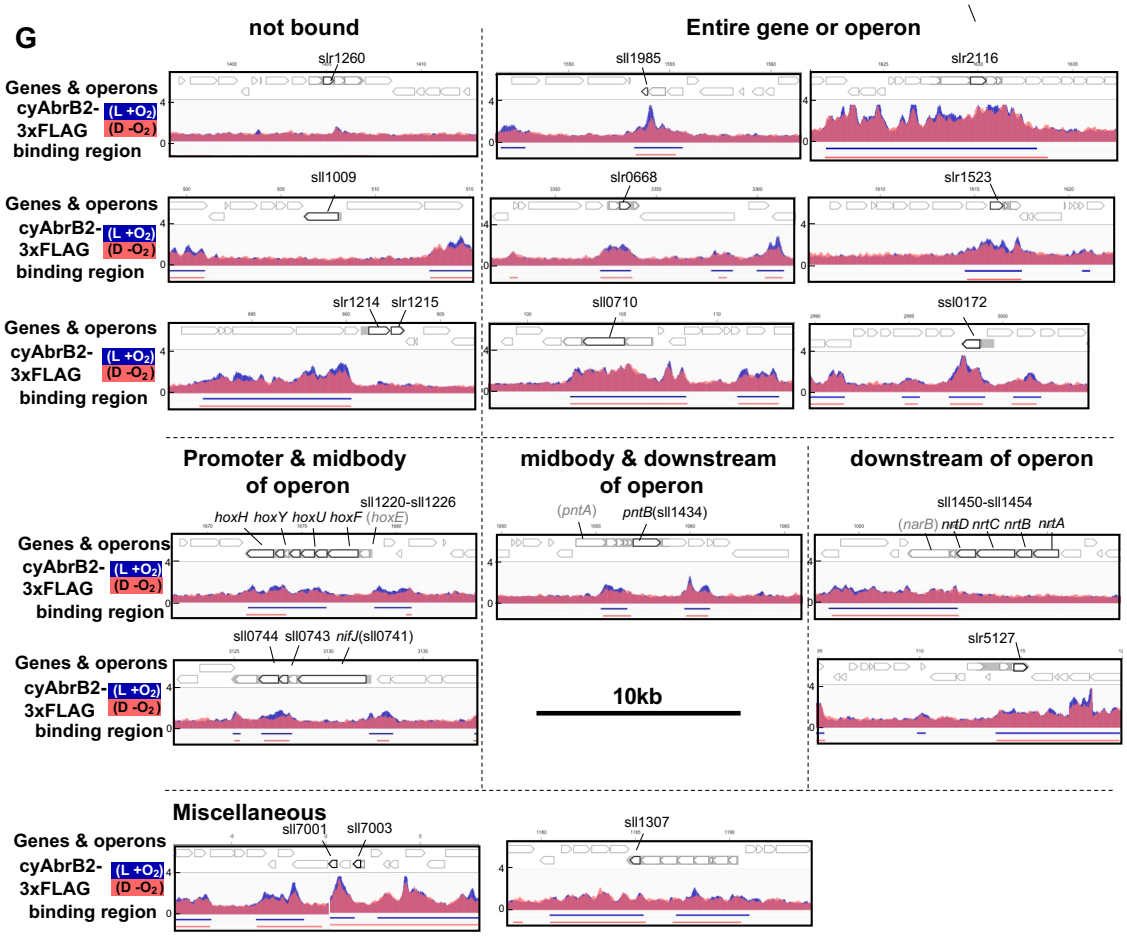

Figure 3

(A) Snapshot of ChIP-seq data for cyAbrB2 and cyAbrB1 under aerobic conditions. The heatmap in the second column indicates expression fold change upon Δ*cyabrb2* under aerobic conditions. Positive values (colored in red) indicate that the gene expression is higher in wildtype than in Δ*cyabrb2*, and negative values (colored in blue) indicate the opposite. The third column indicates the positions for the insertion elements. The heatmap in the fourth column indicates GC contents. High GC content are colored in blue and low GC contents are colored in blue.

601 (B) GC contents and region length of cyAbrB2 binding regions (black dots). The horizontal dotted line

602 indicates the genomic average of GC content.

603 (C) Scatter plot of GC content and binding signal of cyAbrB2. The x-axis is the binding signal of

604 cyAbrB2 in each 100 bp region, and the y-axis indicates GC contents within 500 bp windows sliding

605 every 100 base pairs.

606 (D) Histogram of genes showing the extent of occupancy (not bound, partially overlapped, or entirely

607 overlapped) by the cyAbrB2 binding region. The gray bars indicate non-IS genes, and the count numbers

608 of the non-IS genes are displayed on the gray bars. The black bars indicate the IS genes, and the count

609 numbers of the IS genes are displayed on the black bars.

610 (E) Boxplot showing fold change in gene expression by Δ*cyabrb2* under aerobic conditions. Genes are

611 classified according to the extent of occupancy by the cyAbrB2 binding region. Asterisk (*) denotes

612 statistical significance tested by multiple comparisons of the Wilcoxon-rank test.

613 (F) Fraction of genes overlapped or non-overlapped with cyAbrB2 binding regions at the timepoints of

614 aerobic conditions. Genes are classified according to Figure 1C. Asterisk (*) denotes statistically

615 significant enrichment compared with all upregulated genes tested by multiple comparisons of Fisher's

616 exact test.

617 (G) Distribution of cyAbrB2 around transiently upregulated genes. ChIP-seq data in aerobic (L + O_2) and

618 dark microoxic (D − O_2) conditions are overlayed. Arrows with bold lines indicate transiently upregulated

619 genes. Shaded arrows indicate operons whose data were obtained from a previous study. The bars below

620 the graph indicate the binding regions of each protein. The black bar at the top of the figure indicates a

621 length of 10 kbp.

622

Figure 4

A

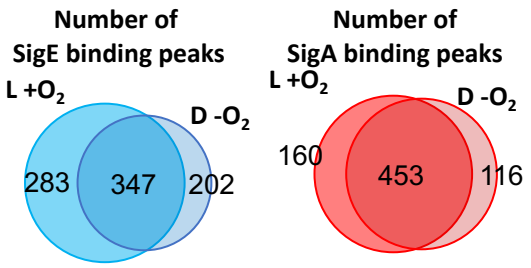

C

		no SigE summit	SigE summit
cyAbrB2	free	1071	598
	bound	280	32
Odds ratio	0.205	p-value	< 2.2e-16

		no SigA summit	SigA summit
cyAbrB2	free	1105	564
	bound	263	49
Odds ratio	0.365	p-value	3.95e-11

B

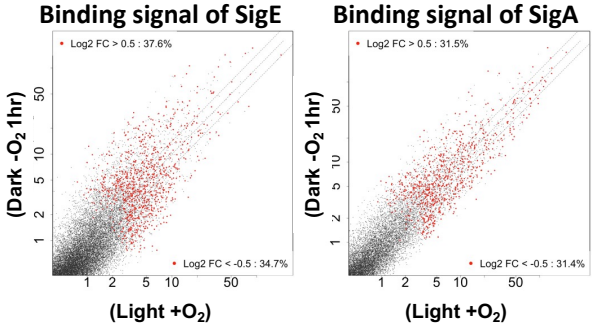

D

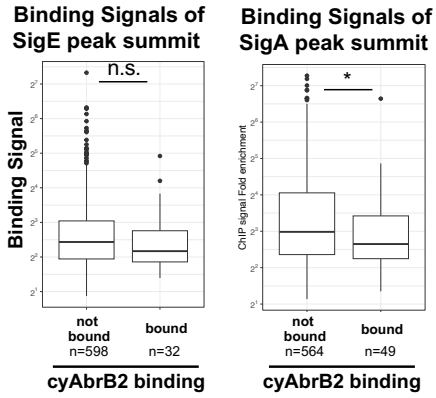

E

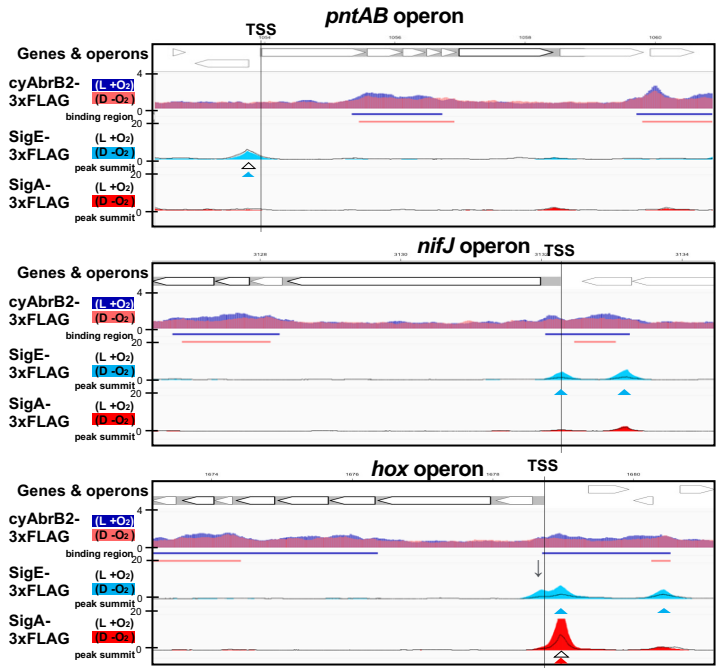

623

624 **Figure 4**

625 (A) Venn diagram showing the number of peaks of SigE (left) and SigA (right) in aerobic (L + O_2) and

626 dark microoxic (D − O_2) conditions. (B) Scatter plot showing changes in the binding signal of SigE and

627 SigA by 1 hour cultivation under microoxic conditions. The binding signal of each 100 bp window is

628 plotted. The binding signals are plotted in Figure 3E. (C) 2x2 tables showing co-occurrence of cyAbrB2

629 bindingregions and SigE peaks (top) or SigA binding peaks (bottom). Odds and p-values were calculated

630 by Fisher's exact test. (D) Distribution of ChIP enrichment signals of SigE and SigA peaks. The peaks

631 were classified into two based on whether they overlapped with the CyAbrB2-binding region. (E)

632 Snapshots of ChIP-seq data for CyAabrB2, SigE, and SigA at the *nifJ* region (top) and *hox* region

633 (bottom). ChIP-seq data for CyAbrB2, SigE, and SigA under aerobic and dark microoxic conditions are

634 overlayed. ChIP-seq data of CyAbrB2 under aerobic and microoxic conditions are colored blue and pink,

635 respectively. ChIP-seq data for SigE and SigA are shown in solid lines (aerobic conditions) and filled

636 lines (microoxic conditions). The positions of TSSs were obtained from a previous study (Kopf et al.,

637 2014) and indicated by vertical dotted lines. Open triangles indicate peak summits under aerobic

638 conditions, and solid triangles indicate peak summits under microoxic conditions.

Figure 5

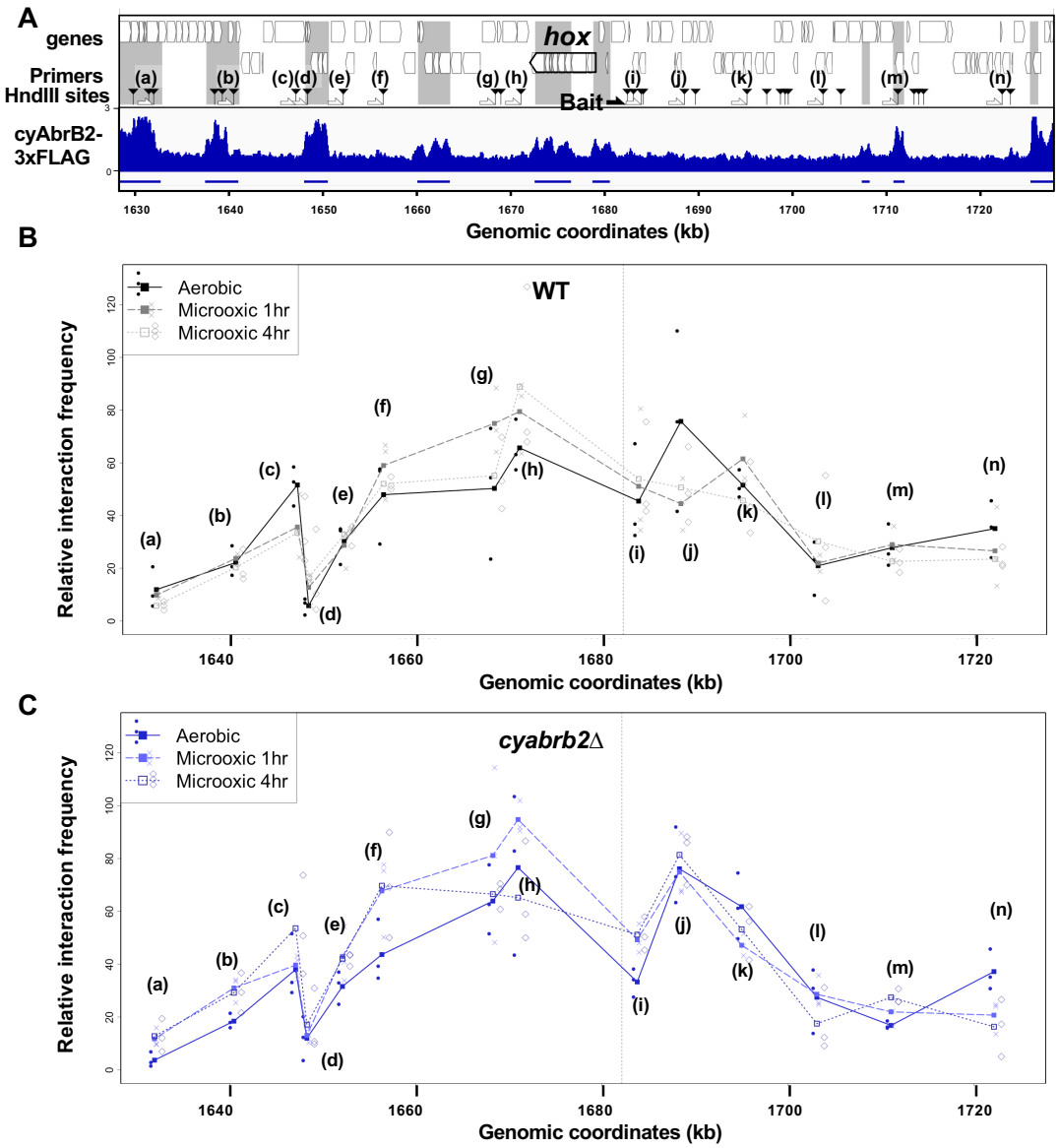

Figure 5 (continuing)

Figure 5 (continued)

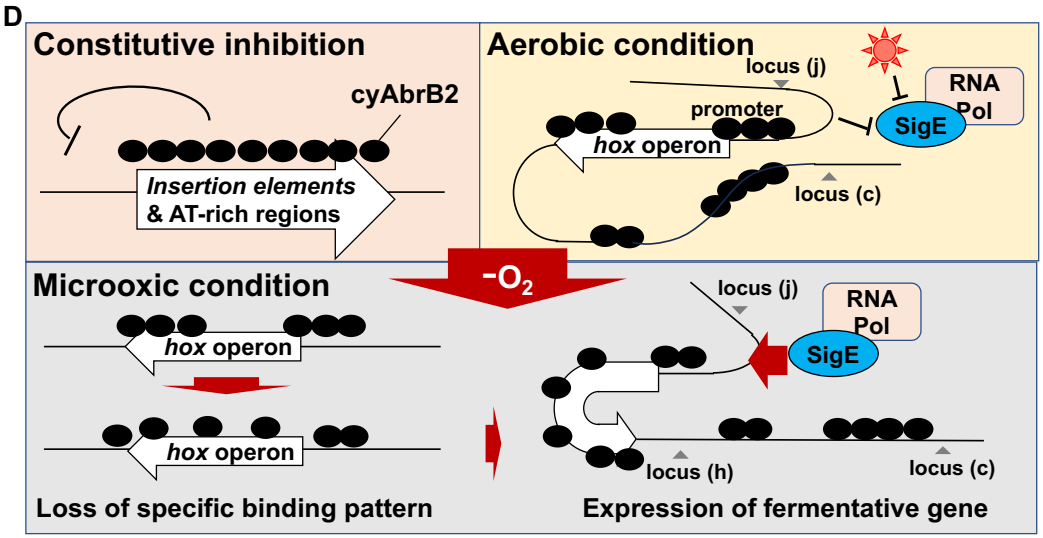

Figure 5

(A) Schematic diagram of 3C analysis around *hox* operon. The black arrow shows the localiton of the bait primer, and white arrows ((a) to (n)) indicate loci where the interaction frequency with bait were assayed. Black arrowheads indicate the position of HindIII sites. ChIP-seq data of cyAbrB2 in the aerobic condition is displayed in the bottom, and cyAbrB2 binding regions are marked with shade. (B) and (C) The line plot showing the interaction frequency of each locus with *hox* fragment in the wildtype (B) and Δ*cyabrb2* (C). The solid, dashed, and dotty lines indicate data in the aerobic condition, 1hr, and 4hr cultivation of microoxic conditions, respectively. The line plots indicate the average interaction frequency over the random ligation (n=3). Indivisual data are plotted (D) Schematic diagram of the dynamics of transcription factors governing fermentative gene expression.

657

Figure S1

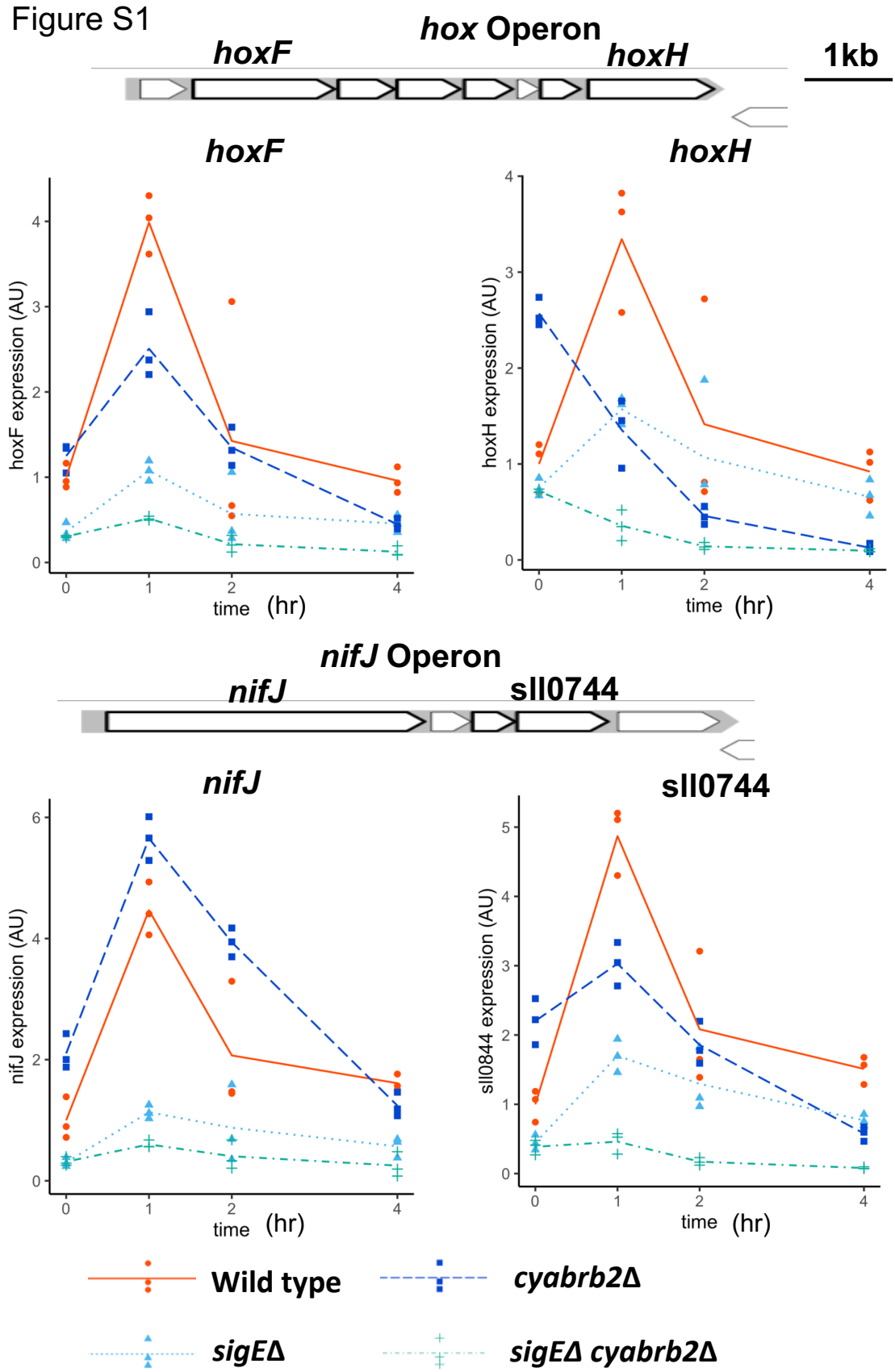

658

659 **Figure S1**

660 RT-qPCR validated the transiently upregulated genes classified by RNAseq. Transcripts extracted

661 from wildtype (solid line), *sigE*Δ mutant (dotty line), *abrb2*Δ mutant (dashed line), and *sigE*Δ

662 *abrb2*Δ double mutant (dot-dashed line) were assayed in the aerobic condition (0hr) and 1,2,4 hour

663 incubation of microoxic conditions. As the representative of the transiently upregulated genes,

664 expression of *hoxF*, *hoxY, nifJ,* and *sll0744* were quantified by RT-qPCR. The line represents the

665 mean of n=3, and individual data points are shown as dot plots. Data of each gene is normalized by

666 the mean score of wildtypes in the aerobic condition.

Figure S2

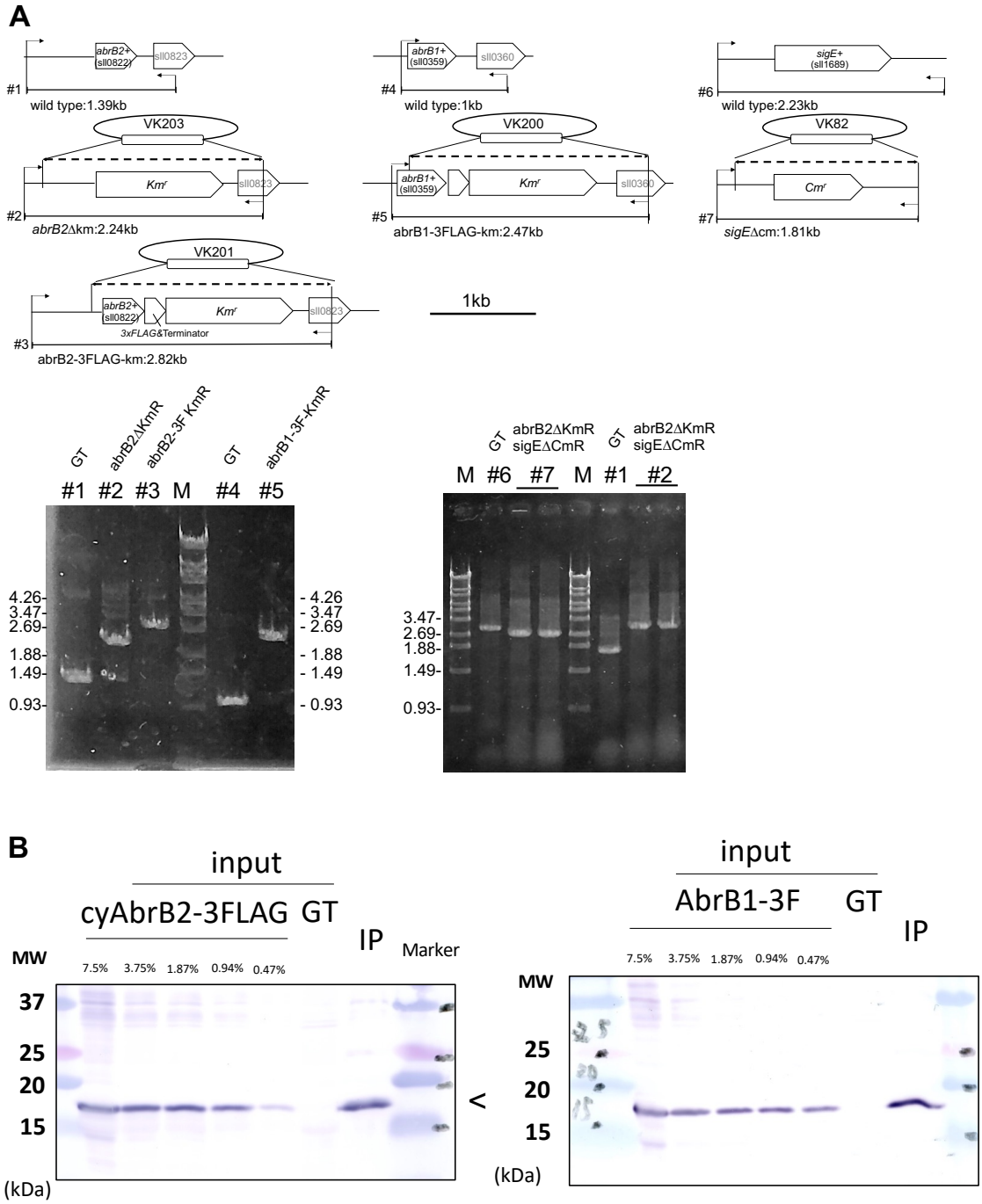

Figure S2 (continuing)

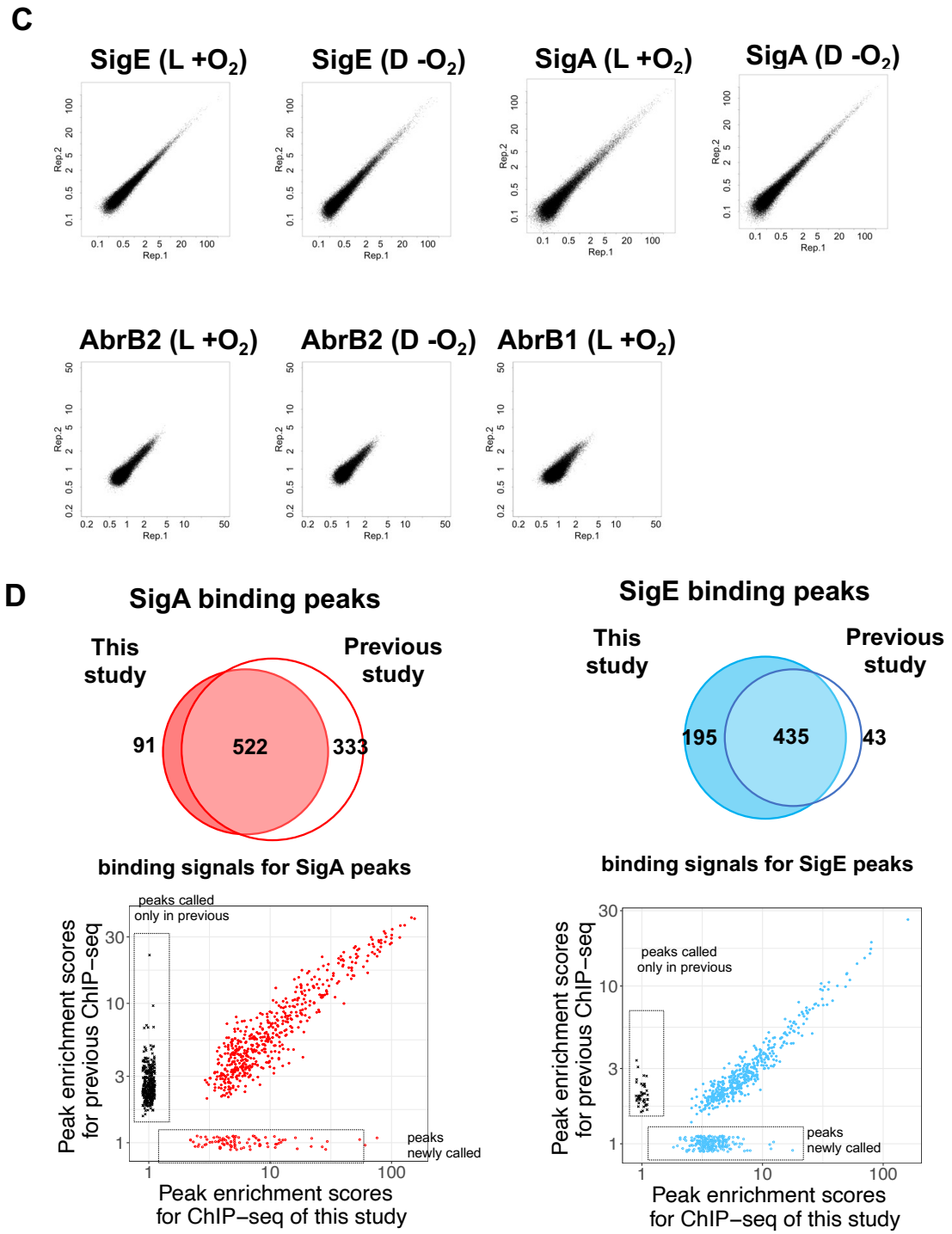

Figure S2

Validation of procedure for ChIP-seq of flag-tagged cyAbrB2, SigE, and SigA.

(A) Confirmation of genomic deletion and the epitope tagging of *abrB2* (#1-#3), the epitope tagging

673 of *abrB1* (#4 and #5), and deletion of *sigE* (#6 and #7). Dotty lines are homologous regions between

674 plasmids and the genome. Arrows indicate position of check primers. (B) The immunoblot for inputs

675 and immunoprecipitants of ChIP for cyAbrB2-FLAG and cyAbrB1-FLAG. Inputs equivalent to the

676 indicated portion of IP were loaded. (C)Scatter plots showing the reproducibility of two replicates

677 for ChIP-seq assay. ChIP-seq data of SigE, SigA, and cyAbrB2 in aerobic and microoxic conditions

678 and ChIP-seq data of cyAbrB1 in the aerobic condition are shown. Dots indicate normalized IP read

679 count / normalized input read count in each 100bp window. X-axis is the value of replicate1, and Y-

680 axis is the value of replicate 2. (D) Reproducibility of ChIP-seq data of SigA and SigE, compared

681 with the previous study (Kariyazono and Osanai 2022). (top) Pie charts show the overlapping of

682 peaks called in this study and the previous study. (bottom) Scatter plot comparing ChIP binding

683 signals of SigA and SigE peaks commonly called in present and previous studies. Plots boxed by

684 dashed lines are peaks called only in the present or previous study.

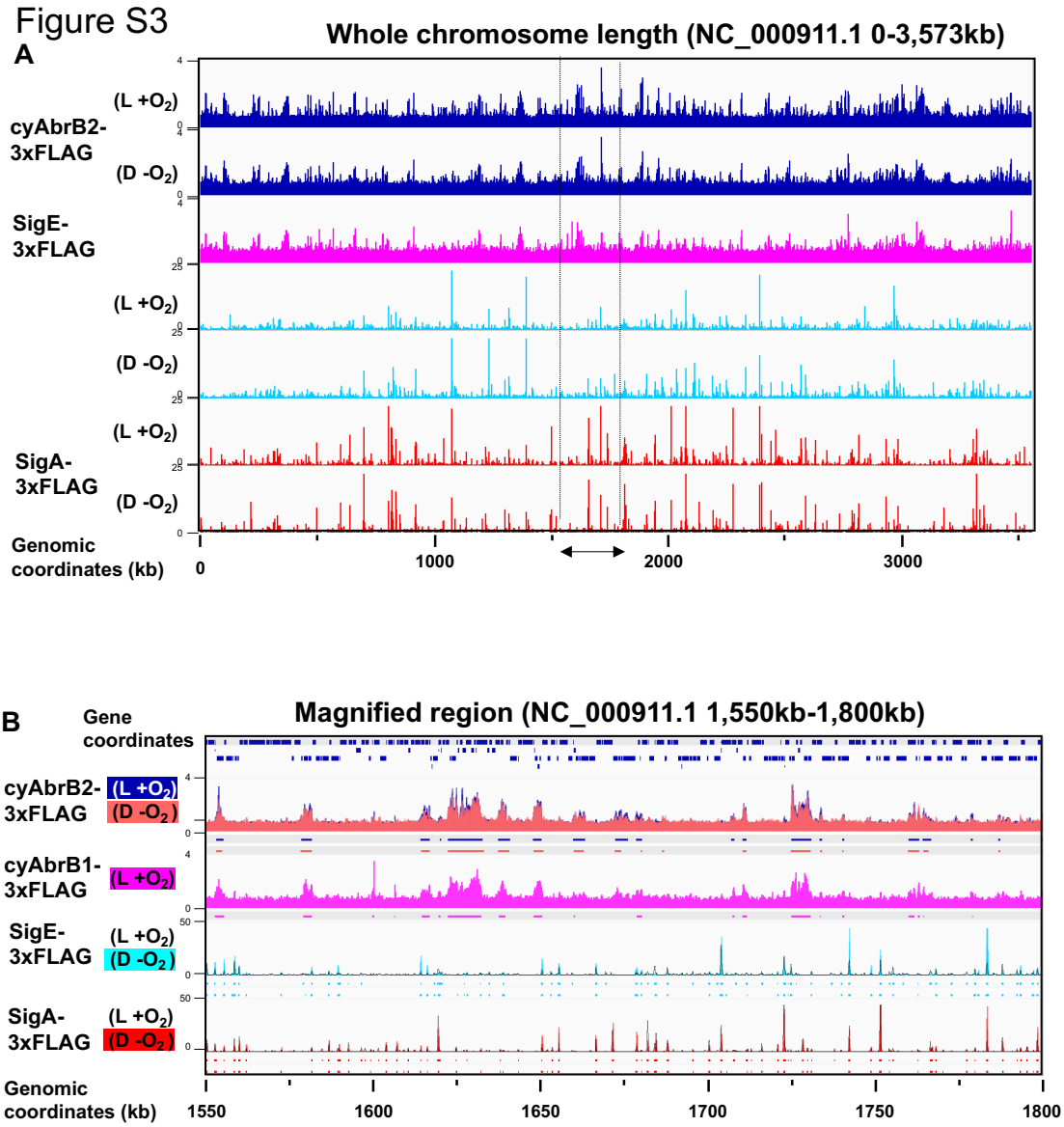

Figure S3

Overview for ChIp-seq of flag tagged cyAbrB2, cyAbrB1, SigE, and SigA. Y-axis indicates [normalized IP read count / normalized input read count at each 25bp window], and X-axis indicates chromosome position.

(A) Distribution of cyAbrB2, cyAbrB1, SigE, and SigA across the whole genome of *Synechocystis*. Aerobic (L +O_2) and dark microoxic (D -O_2) data are displayed. (B) Magnified image for

692 chromosome position of 1,550kb-1,800kb. ChIP-seq data of cyAbrB2, cyAbrB1, SigE, and SigA in

693 aerobic and dark microoxic conditions are overlayed. The dots below the graph indicate the binding

694 region of each protein calculated by peak caller.

695

Figure S4

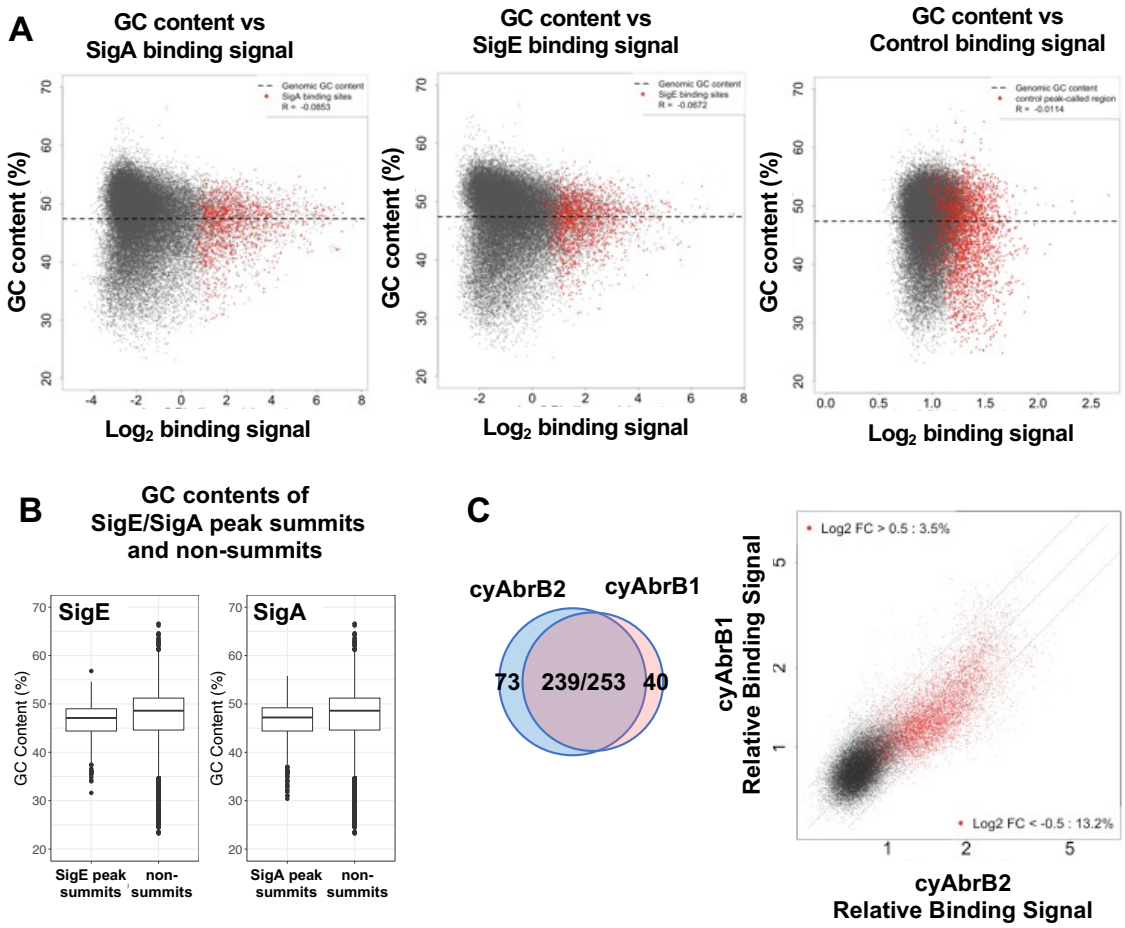

Figure S4

(A) Scatter plot showing GC contents in each 100bp vs. binding signal of SigA, SigE, and control IP. Data are displayed as in Figure 3C. (B) GC content in each 100bp of (left) SigE peaks and non-SigE peaks, and (right) SigA peaks and non-SigA peaks. (C) Venn diagram showing overlap of the binding region of cyAbrB1 and cyAbrB2 (left), and scatter plot showing ChIP binding signal of cyAbrB2 (y-axis) and cyAbrB1(x-axis) in the aerobic condition. Data is plotted as in Figure 4E.

Figure S5

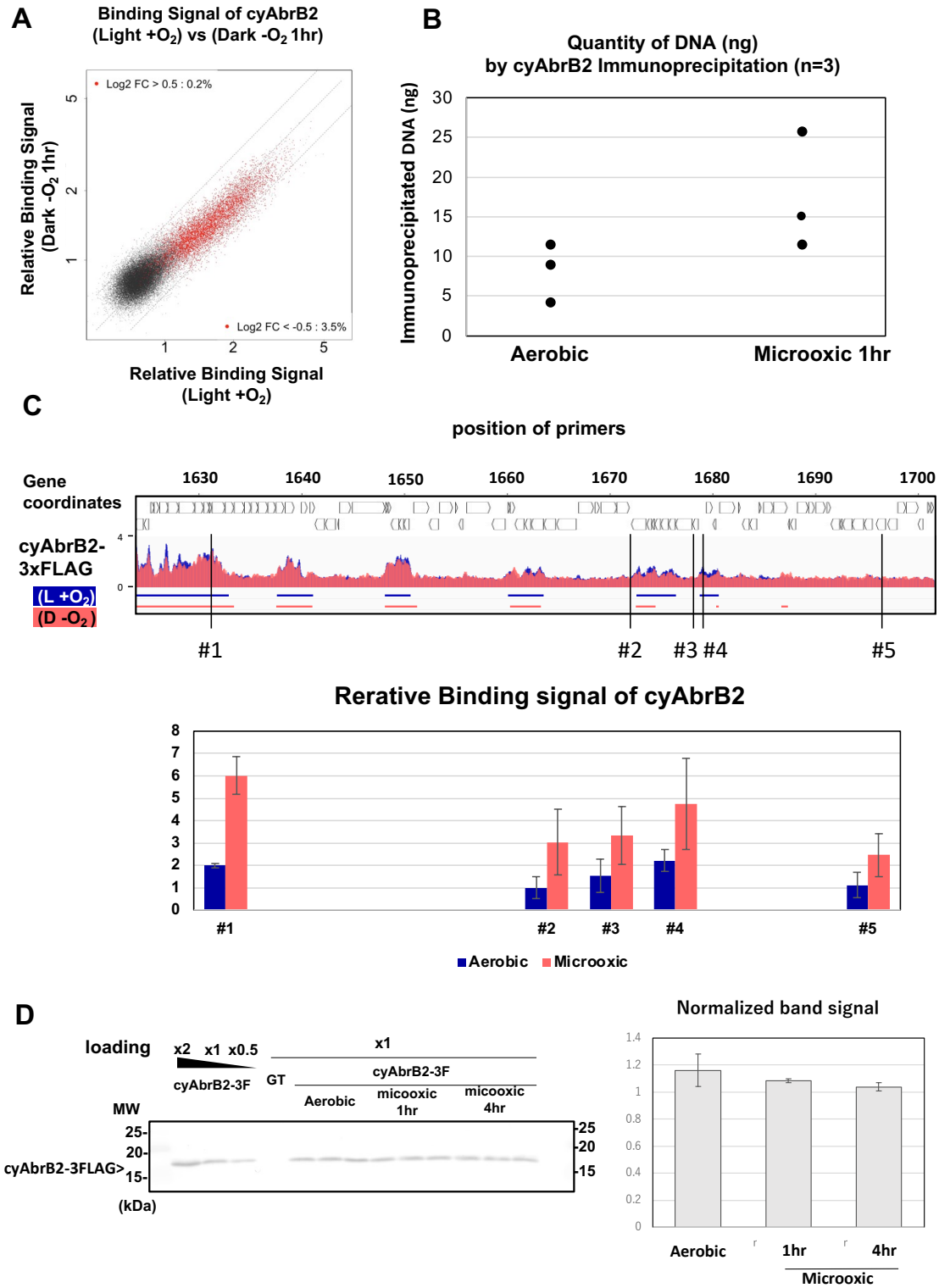

Figure S5(continuing)

706 **Figure S5**

707 (A) Scatter plot showing changes of the binding signal by 1hr cultivation in the microoxic condition.

708 The binding signal of each 100bp window is plotted. Red dots are cyAbrB2 binding regions in either

709 aerobic or microoxic conditions. The dotty lines indicate Log2 fold enrichment of 0.5, 0, -0.5

710 between aerobic and microoxic conditions. (B) Amount of precipitated DNA by cyAbrB2 ChIP.

711 Three experiments were performed in the aerobic and microoxic conditions. (C) Quantification for

712 ChIP of cyAbrB2 by qPCR. The position of primers and ChIP-seq data of cyAbrB2 are shown at the

713 top. (D) Western blot images of cyAbrB2-3FLAG. Proteins were extracted in the aerobic condition

714 and 1hr and 4hr incubation under microoxic conditions. The total protein concentration of each

715 sample was adjusted to 4mg/mL, measured by the BCA method. Quantification of cyAbrB2 from

716 western blot image was performed by ImageJ (ver. 2.0.0-rc-65) and plotted in the right graph.

717

Figure S6

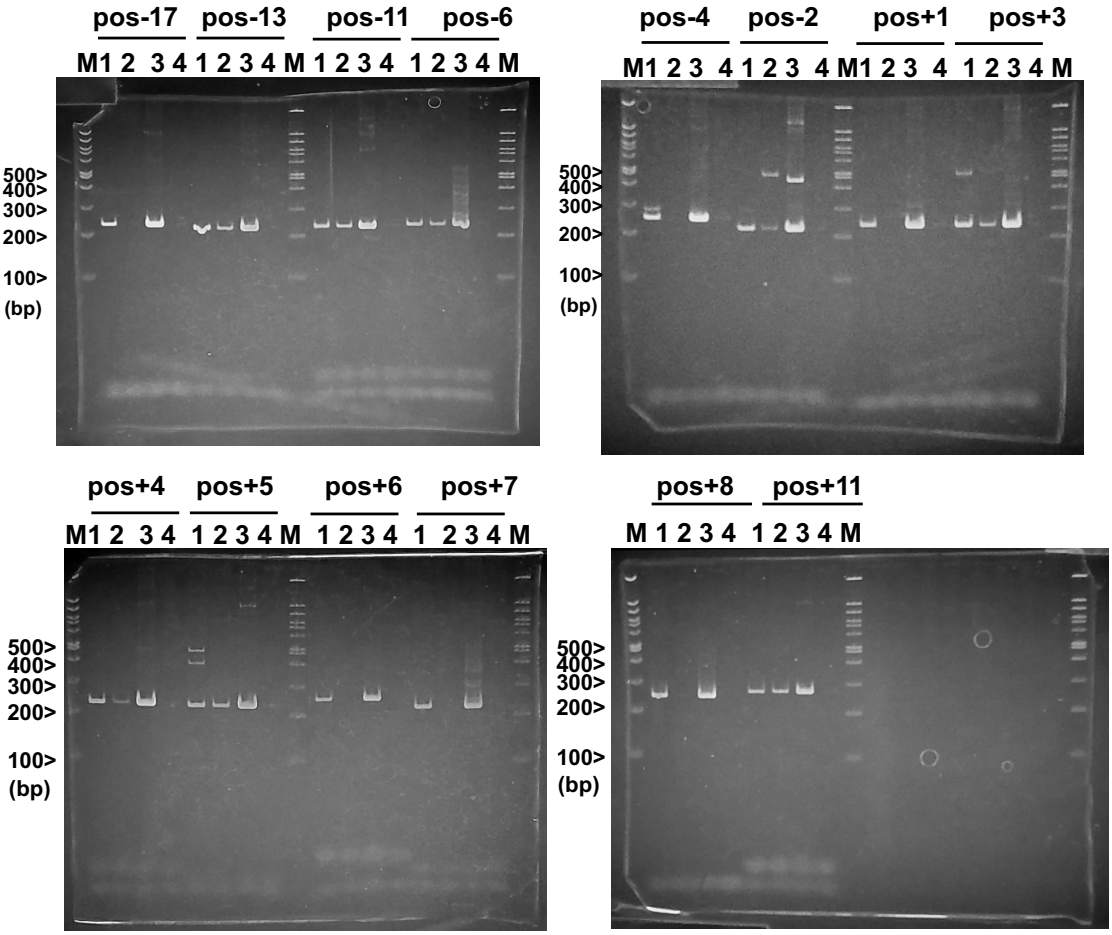

M:100bp ladder (DM2100 SMOBIO)
1 Calibration sample x500
2 Calibration sample x2500
3 3C sample x100
4 Unligated sample x100

GoTaq® Hot Start Program

95˚C 2min
95˚C 15sec | **x35**
60˚C 30sec
4˚C Hold

Figure S6

The validation of unidirectional primer sets for 3C assay is shown in Figure 5. The 3C sample in this assay is the mixture of all 3C samples assayed in Figure 5.

Figure S7

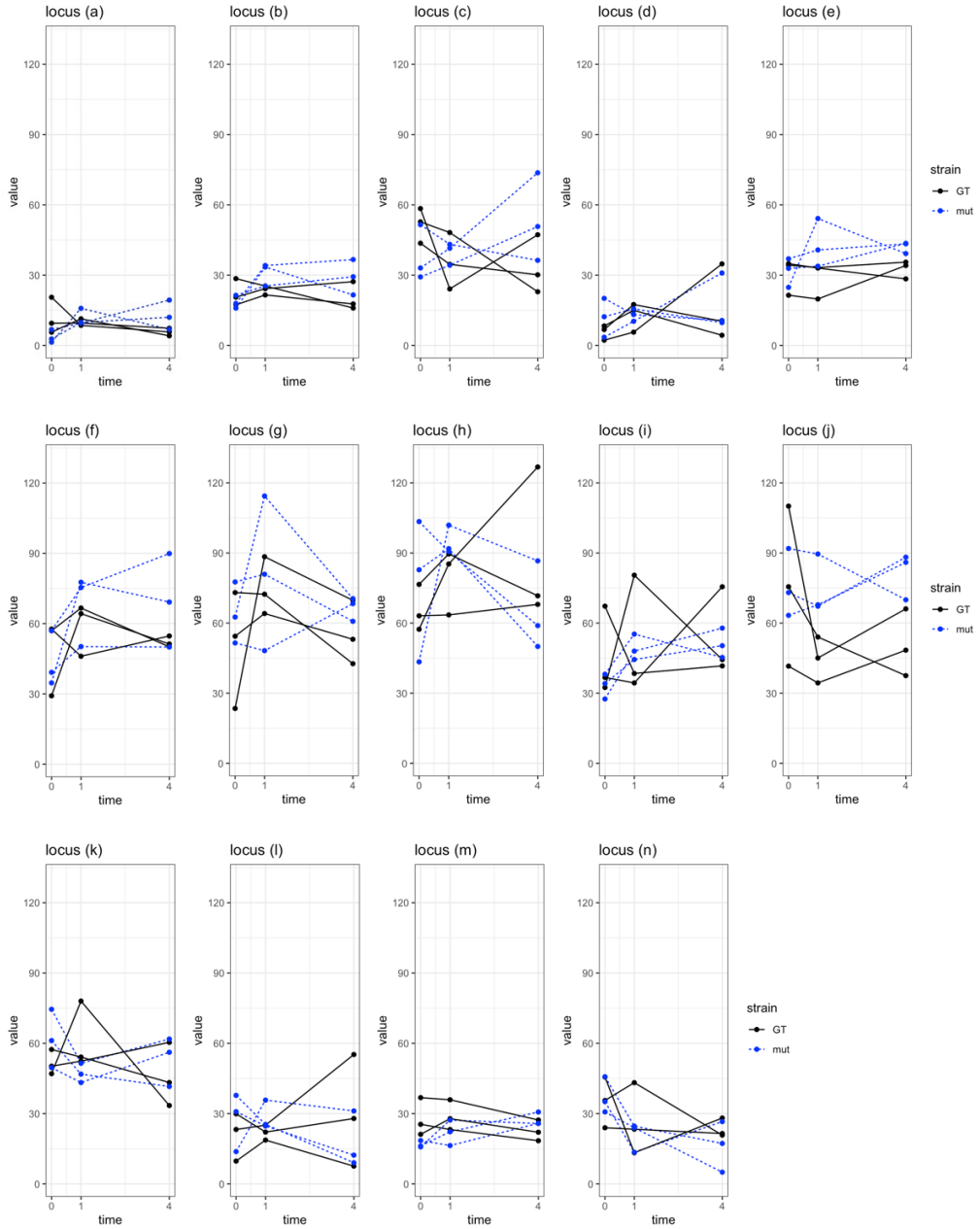

Figure S7

Re-plotting of Figure 5B and 5C with the x-axis showing time (0,1,4 hr in microoxic conditions) and the y-axis showing the interaction frequency. Plots from the individual samples are connected by solid (Wildtype) or dotty (*cyabrb2*Δ) lines.

727 **Table S1 Fold changes of transcripts from *sigA, sigB, sigC, sigD, and sigE***

		0hr vs 1hr		1hr vs 4hr	
Sigma factor	**locus**	**Log2FC**	**FDR**	**Log2FC**	**FDR**
SigA	slr0653	-0.873248	0.00766486	-0.0013514	0.99797563
SigB	sll0306	1.38098826	8.42E-06	0.77453605	0.04057775
SigC	sll0184	2.97101055	1.75E-16	1.30743549	0.00067892
SigD	sll2012	0.4701823	0.1498473	-0.4522181	0.32402556
SigE	sll1689	-1.9111759	1.96E-11	-1.1223298	0.00633142

728 Data is extracted from Supplemental Table S7.

729

730 **Table S2 List of strains used in this study**

Strain ID	**Host strain**	**genotype**	**Reference**
GT			Williams, 1988
G50	GT	*sigE*ΔkmR	T. Osanai, et al,2005
KR93	GT	SigA-8His-kmR	(Kariyazono and Osanai 2022)
KR94	GT	SigA-3FLAG-kmR	(Kariyazono and Osanai 2022)
KR340	GT	*abrB2*ΔKmR	in this study
KR338	GT	AbrB(sll0359)-3xFLAG-KmR	in this study
KR339	GT	AbrB2(sll0822)-3xFLAG-KmR	in this study
KR359	KR340	*abrB2*ΔKmR *sigE*ΔCmR	in this study

731

732 **Table S3 plasmids used in this study**

Plasmid ID		**backbone**	
VK82	*sigE*ΔCmR	pTA2 (Toyobo)	transformation for KR359
VK200	AbrB1-3F-KmR	pTA2 (Toyobo)	transformation for KR338
VK201	AbrB2-3F-KmR	pTA2 (Toyobo)	transformation for KR339

VK203	*abrB2*ΔKmR	pTA2 (Toyobo)	transformation for KR340

733

734 **Table S4 oligonucleotides used in this study**

Oligonucleotides ID		**sequence**
qPCR_hoxF_F	Figure S1	GTCATCTGCAATGCTGACGAA
qPCR_hoxF_R	Figure S1	CCAACACACTGCGGTCCAT
qPCR_hoxH_F	Figure S1	TCCCGTTACCCGGATTGA
qPCR_hoxH_R	Figure S1	GCCCTGGTCGTTGAGGAAA
qPCR_nifJ_sll0741_F	Figure S1	GATTCGGGGCAAAGTTTACG
qPCR_nifJ_sll0741_R	Figure S1	TACCTGGATGGTGAACTTAG
qPCR_sll0744_F	Figure S1	GCAGCTTAAATGGTTCTACC
qPCR_sll0744_R	Figure S1	CCAAATCTGTGGGTACGTAG
qPCR_nrpB_F	Figure S1	AAAGGGTAAGGGTGCAAAGG
qPCR_nrpB_R	Figure S1	AATTCCTCAAGCGGTTCCAC
new_abrB_0822_del_chkF	Figure S2A	AATCCTCCGCCAAACTTTG
abrB_0822_tag4	Figure S2A	GGAGTTTTCACCATCAGTC
abrB_0359_chkF	Figure S2A	AGAGGGAAAAATTCCTCGGC
abrB_0359_tag4	Figure S2A	TCGCCAGGGAAAGTAATTGG
SigE_whole_del_chkF	Figure S2A	GGAACGCTTGGAATGGCAAC
sigE_tag4	Figure S2A	TGAAGGGGGTAGATTTAAGCC
ChIP_slr2118_F1	Figure S5C #1	CATTTCAAGCGAGATAGCAG
ChIP_slr2118_R1	Figure S5C #2	TGGAAAGTGCCTGTTCAAAG
ChIP_ThoxH_F	Figure S5C #2	CATCACCGAGGGCATATCTAG
ChIP_ThoxH_R	Figure S5C #2	ACATAAGGCTATGGAAACC
ChIP_pHox_2F	Figure S5C #3	ACAGAGGATGGACAAATGTC
ChIP_pHox_2R	Figure S5C #3	TACCGCTTCGTCATTCTGCT
ChIP_pHox_up_2R	Figure S5C #4	TCGATTACTTCCCTTTAGTG
ChIP_pHox_up_2F	Figure S5C #4	CTTCGGCTCCATGTATTC
ChIP_sll0814_F	Figure S5C #5	GTTACTACCGCTATCTATCG
ChIP_sll0814_R	Figure S5C #5	ATGACGTAAACCGGCTCTGAC

3Chox_Hcommon	Figure 5	CGGTCCCTTTGGACGTAATC
3Chox_H01_pos_+1	Figure 5	GGGTTGGGCGCAACATTAAG
3Chox_H02_pos_+3	Figure 5	CAAAGCGATTTTGGCTGGTG
3Chox_H03_pos_+4	Figure 5	GATGTGGTGGAAGATACGGAC
3Chox_H04_pos_+5	Figure 5	GGAGCCACAGGGGAATTTAAC
3Chox_H05_pos_+6	Figure 5	GGTCAGATTTTATTGGTTGCATGG
3Chox_H06_pos_+7	Figure 5	TTGTCAATGTCAACCGCAAC
3Chox_H07_pos_+8	Figure 5	TTATTGCCCAATCTGGCGAC
3Chox_H08_pos_+11	Figure 5	AGGCAAGACAGATAAACCTTCTG
3Chox_H09_pos_-2	Figure 5	GGGGCATAGGGAGCAAACC
3Chox_H10_pos_-4	Figure 5	GGGGTAGTACCGGAAGTGG
3Chox_H11_pos_-6	Figure 5	TTGGGCTGATTCTTGCAATTC
3Chox_H12_pos_-11	Figure 5	AGCTTTTGTCTAACACCGTATCG
3Chox_H13_pos_-13	Figure 5	AAGCCATCCTTCAAAACCCG
3Chox_H14_pos_-17	Figure 5	GCCCCATCGGTGAGAAAAAG
qPCR_hoxF_F	Figure 5 (internal control)	GTCATCTGCAATGCTGACGAA
qPCR_hoxF_R	Figure 5 (internal control)	CCAACACACTGCGGTCCAT